

COMPUTATIONAL AND GROUND BASED EXPERIMENTAL INVESTIGATIONS OF THE EFFECTS OF SPECIFIED AND UNSPECIFIED (FREE) PRESSURE CONDITIONS AT CONDENSER EXIT FOR CONDENSING FLOWS IN TERRESTRIAL AND MICRO-GRAVITY ENVIRONMENTS

Amitabh Narain¹, Shantanu Kulkarni, Soumya Mitra, Jorge H. Kurita
and Michael T. Kivisalu

Department of Mechanical Engineering-Engineering Mechanics
Michigan Technological University
Houghton, MI-49931

ABSTRACT

Reported experimental and computational results confirm that both the flow features and heat transfer rates inside a condenser depend on the specification of inlet, wall, *and* exit conditions. When exit pressure is changed from one steady value to another, the changes required of the interior vapor flow towards achieving a new steady duct flow are such that they do not demand removal of the new exit pressure imposition back to the original steady value. This behaviour of condensing flow is unlike that of any incompressible single phase duct flow which cannot allow imposition of an exit pressure other than the “required” value. Instead, new steady flows may be achieved for different steady exit pressure prescriptions (termed category I flows) through appropriate changes in the vapor/liquid interfacial configurations and associated changes in interfacial mass, heat transfer rates (both local and overall), and other flow variables. This special feature of these flows is for the commonly occurring large heat sink situations for which the condensing surface temperature (not heat flux) remains approximately the same for any given set of inlet conditions while exit condition changes. In this paper’s experimental context of flows of a pure vapor that experiences film condensation on the inside walls of a vertical tube, the reported results provide important quantitative and qualitative understanding. The theoretical and experimental results presented in this paper allow us to propose important exit-condition based categorization of these flows. Of these, category II flows, which are defined to be the cases for which exit pressures are left unspecified, have typically been assumed to hold for most actual steady realizations of gravity driven flows. However it is shown here that steady flows under self selected exit pressure conditions are achieved under these conditions only if special hardware arrangements are made that allow vapor to freely choose an exit pressure. If this is not so, one often has an inadvertent category I flow without the explicit knowledge of the imposed exit pressure condition. It is theoretically shown here that though this category II flow situation in the absence of specification of exit condition constitutes an “ill posed” steady boundary value problem, steady flows may still be experimentally realized under special arrangements. This fact is also validated by unsteady theory which shows that solutions from many different initial conditions may tend to a unique steady attracting solution (as $t \rightarrow \infty$) for *some* of the internal and/or external flows. These “attractors” exist and are strong for gravity driven flows and are often weak to non-existent for zero gravity or horizontal shear/pressure driven flows (both for internal and external flows). In microgravity, the “attractors” for category II internal flows are weak in the sense that they significantly lose their strength of “attraction” after a certain downstream distance – after which the flows are indeterminate if exit pressure remains unspecified. For these microgravity situations, the remedy is to run condensers under suitably specified inlet and exit pressures (category I conditions) as well as a proper cooling strategy (i.e. proper wall temperature variations).

Key-words: film condensation, phase-change heat transfer, two-phase flows, interfacial waves.

¹To whom correspondence should be addressed. E-mail: narain@mtu.edu, Phone: 906-487-2555 Fax: 906-487-2822

NOMENCLATURE

C_{p1}	Specific heat of the liquid condensate, J/(kg-K)
C_{p2}	Specific heat of the vapor, J/(kg-K)
D	Inner diameter of the test-section, m
G	Inlet mass flux, $4 \cdot \dot{M}_m / (\pi \cdot D^2)$, kg/(m ² /s)
$h_{fg}(p_{in})$	Heat of vaporization at pressure p_{in} , J/kg
\bar{h}	Average heat transfer coefficient, $\dot{Q}_{out} / (\pi \cdot D \cdot L)$, W/(m ² -K)
h	Channel gap, m
Ja	Condensate Jakob number, $C_{p1} \cdot \bar{\Delta T} / h_{fg}(p_{in})$
Ja_{LV}	Vapor Jakob number, $C_{p2} \cdot \Delta T_{sup} / h_{fg}(p_{in})$
k_1	Conductivity of condensate liquid, W/(m-K)
L	Length of the test-section, m
L_C	Characteristic length, $L_C = D$ for tubes and $L_C = h$ for channels, (m)
\dot{M}_m	Vapor flow rate at test-section inlet, g/s
\dot{M}_L	Liquid flow rate at test-section exit, g/s
\dot{M}_V	Vapor flow rate at test-section exit, g/s
p_B	Evaporator (boiler) pressure, kPa
p_{D2}	Pressure at the location near the rotameter, kPa
$p_{T''}$	Pressure at a location downstream of the test section, kPa
p_{in}	Pressure at the test-section inlet, kPa
p_{exit}	Pressure at the test-section exit, kPa
Pr_1	Condensate liquid Prandtl number, $\mu_1 \cdot C_{p1} / k_1$
p_{xi}	Test-section pressures at different locations $x = x_i$ ($i = 1, 2, \dots$), kPa
\bar{q}	Average convective heat flux, W/m ²
\dot{Q}_b	Net heat rate into the evaporator, W
\dot{Q}_{out}	Net heat rate out of the test-section, W
Re	Inlet vapor Reynolds number, $4 \cdot \dot{M}_m / (\pi \cdot D \cdot \mu_2)$
T_B	Evaporator fluid temperature, °C
T_R	Rotameter fluid temperature, °C
$T_{sat}(p)$	Saturation temperature at pressure p , °C
T_{s-xi}	Condensing surface temperatures at different locations $x = x_i$ ($i = 1, 2, \dots$), °C
\bar{T}_w	Mean condensing surface temperature, °C
$T_w(x)$	Non-uniform steady condensing surface temperature, °C
T_{V-in}	Vapor temperature at test-section inlet, °C
T_{C-in}	Temperature of the counter-current coolant water flow at the approach to the test-section, °C
u	Non-dimensional velocity in the x-direction
U	Velocity in the x-direction, m/s
u	Dimensional velocity in x-direction, m/s
v	Non-dimensional velocity in y-direction
v	Dimensional velocity in y-direction, m/s
x	Non-dimensional distance in x direction (x/L_C)
x_e	Ratio of test section length to characteristic length (L/L_C).

x	Distance in x direction, m
x_{fc}	Approximate length needed for full condensation (estimated by computations), m
y	Non-dimensional distance in y direction (y/L_C)
y	Distance in y direction, m
$\overline{\Delta T}$	$T_{sat}(p) - \overline{T}_w$, °C
ΔT_{sup}	Vapor superheat, $T_{V-in} - T_{sat}(p)$, °C
Δp	$p_{in} - p_{exit}$, kPa
Z_e	Ratio of exit vapor mass flow rate to total inlet mass flow rate
$Z(x)$	Ratio of vapor mass flow rate to total mass flow rate at any location x along the test section
δ	Non-dimensional value of condensate thickness
ρ_2	Density of vapor, kg/m ³
ρ_1	Density of liquid, kg/m ³
μ_2	Viscosity of vapor, kg/(m-s)
μ_1	Viscosity of liquid, kg/(m-s)
D_τ	Transient decay time for disturbances, s

Subscripts

Exit	Test-section exit
In	Test-section inlet
Na	Natural steady case
Exp	Obtained from experiments
comp	Obtained from computations

1. INTRODUCTION AND BACKGROUND

This paper presents a synthesis of results obtained from a fundamental and novel experimental investigation (see Narain et al. [1]) of effects of exit conditions on internal condensing flows and computational investigations ([2]-[6]) of internal and external condensing flows. In section-6, the paper also presents a new set of generalized results for this and other internal two-phase flows. Reported experimental results confirm the existing computational results for internal condensing flows ([4], [5], [6]) that both the flow features and heat transfer rates inside a condenser depend on exit pressure conditions over and above inlet and wall conditions (i.e., the method of cooling for the condensing surface). The steady condensing surface temperature (not heat flux) variation is assumed fixed and known or knowable (through consideration of the appropriate conjugate problem). This paper identifies and establishes a multiplicity of steady/quasi-steady solutions – and/or oscillatory flows – under different steady conditions at the exit. Experiments support the existing simulation results ([4], [5], [6]) that have already shown, among other results, the presence of multiple steady/quasi-steady solutions under multiple steady specifications of the exit condition. The condenser exit condition (for partial as well as full condensation) is specified by exit pressure. For partial (incomplete) condensation flows, specification of exit pressure is equivalent (see Fig. 6 in [4]) to specification of exit vapor quality i.e. the ratio of vapor mass flow rate at the exit to the inlet mass flow rate (see simulation results from [4]-[6]). The computational simulations ([4], [5], [6]) for the gravity driven partial condensation cases (such as flows inside a vertical tube) also predict that, for a certain set of inlet and wall conditions, even if the exit condition is not specified and a suitable range of exit conditions is available for the flow to choose

from, the condensate flow under gravity makes the overall flow seek and attain a specific “natural” flow and associated exit pressure condition (in Narain et al. [4] this situation is also termed as a *natural* unspecified steady exit condition due to the presence of an “attractor,” i.e., an “attracting” solution). Unfortunately many planned system designs incorporate a condenser and assume that the condenser will *always* find a “natural” steady flow since no exit conditions are specified. This is not generally true. The attainment of natural steady flows under unspecified exit conditions require special hardware arrangements and, even then, they occur more readily (over a larger parameter zone) for gravity driven condensate flows than they do for shear driven flows (see [2] – [3] and [6]). The reported experimental results for gravity driven partial condensation cases under unspecified exit conditions support the computational results – both qualitatively and quantitatively. Therefore, for an unspecified exit condition flow, the steady “natural” exit condition may or may not exist depending on whether or not a steady “attractor” exists. For example, as shown in [6], an attractor does not exist for many slow to moderate inlet flow rates in horizontal or zero gravity situations. Furthermore even if an “attractor” does exist, its realization depends on whether the attracting “natural” exit pressure value falls within the range of exit pressures made available to the condensing flow test-section by the rest of the system/flow-loop. In the absence of *active* specification of a steady exit condition, the available range of steady exit conditions is determined by the components downstream of the condenser as well as the specific nature of the hardware used in the design of the rest of the system (or flow loop). Furthermore, because of the small pressure drops (see [6] or experimental runs reported here), when a steady “natural” exit condition is achieved under unspecified conditions, or when the specified exit condition is not too far from this “natural” steady exit value, typically, vapor flows are typically close to incompressible.

The vertical in-tube internal partial condensing flows are investigated here for a downflow configuration. Though numerous in-tube condensation experiments have been done, most of the well known in-tube vertical downflow experiments done by Goodykoontz and Dorsch [7]-[8], Carpenter [9], etc. either limit themselves to sufficiently fast flow portions of the duct that do not significantly depend on exit conditions or operate under a particular (natural or otherwise) set of exit conditions (that gets specified or remains unspecified depending on the employed experimental set up) and, therefore, results may vary from one experimental system to another. In addition to our group’s very early (see Yu [10]) and subsequent ([4], [5]) computational findings on the importance of exit conditions for internal condensing flows, experimental findings of Rabas and Arman ([11]) have also indicated the significance of exit conditions through their observation that the presence or absence of valves at the exit affected some of their in-tube vertical downflow results.

Furthermore, several experimental results and analyses ([12] - [19]) indicate that, for certain physical arrangements leading to a specific class of inlet and outlet conditions, transients and instabilities are expected in complete condensation horizontal (or slightly tilted) in-tube internal condensing flows. Since these experiments and the corresponding modeling techniques in the literature limit themselves to a particular type of inlet and exit conditions, they do not directly apply to the presence or absence of observed transients and instabilities in other feasible categories of exit-condition specifications.

In the context of *boundary value* problems for internal condensing flows, what is new is that our computational and experimental results unequivocally show that the commonly occurring condensing flows are very sensitive to the *nature* of exit conditions as well as to the changes in exit conditions (due to changes in exit pressure). This sensitivity arises from the ease with which these changes alter the vapor flow field in the interior. Therefore when only exit pressure condition is changed from one steady value to another, the changes required for the interior vapor flow towards attaining a new steady flow

are such that they do not demand removal of the new exit pressure imposition - as is the case for incompressible single phase duct flows with only one allowed exit pressure. Instead, for condensing flows, new steady flows are achieved for new exit conditions through appropriate changes in the vapor/liquid interfacial configurations and associated changes in interfacial mass, heat transfer rates (both local and overall), and other flow variables. This happens because the “interface tracking equation” (see, e.g., eqn. (20) of [4] which arises from setting the interfacial mass flux \dot{m}_{LK} given in eqn. (A.10) of the Appendix equal to another interfacial mass-flux \dot{m}_{Energy} given in eqn. (A.11) of the Appendix) which locates the interface involves a key parameter \dot{m}_{Energy} . This key parameter \dot{m}_{Energy} which is obtained from the interfacial heat flux associated with the local temperature gradient easily changes with changing interface location; particularly if the interface is near a heat transfer surface at a prescribed wall temperature. It is the absence of an available adjustable range for interfacial mass-flux \dot{m}_{Energy} for single-phase flows (which have no interface) and for adiabatic gas-liquid flows (where this interfacial mass-flux is constrained to be zero) that makes it difficult to externally impose different exit pressures for these better understood flows.

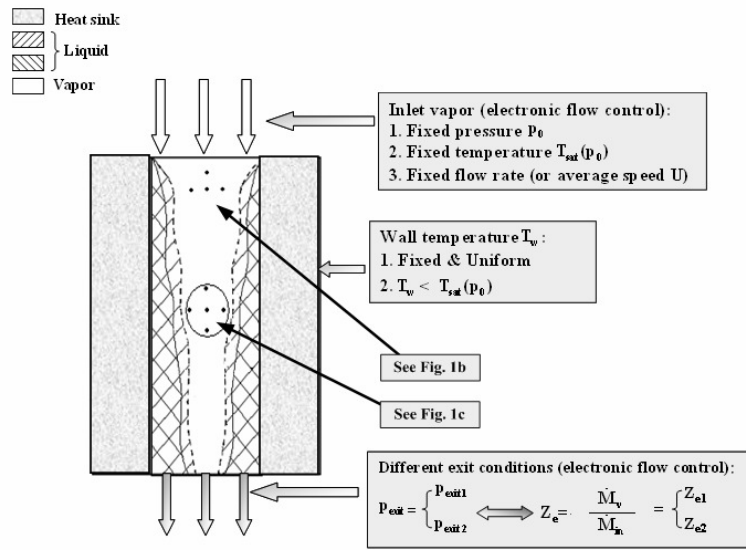


Fig. 1a

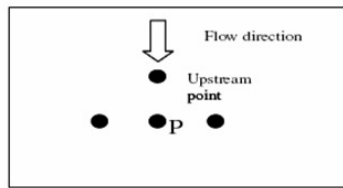


Fig. 1b

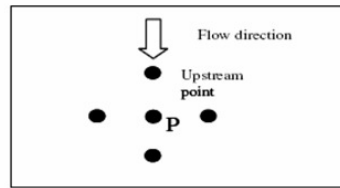


Fig. 1c

Fig. 1: The schematic for the flow through test-section and exit condition issues.

Fundamentally, internal condensing flows’ exit condition sensitivity arises from governing equations being “elliptic” or requiring “two-way” space co-ordinates in the flow direction (i.e. flow variable at a point P is influenced both by upstream and downstream local neighbors as shown in Fig. 1c) to determine the flow fields in the two phases *and* the interface location. However, this sensitivity to exit

conditions, or “two-way” behavior, is *special* and does not result from the typical “ellipticity” associated with slow flows and flow reversals (which are, as described in Patankar [20], associated with the changes in the sign of local Peclet numbers). In fact, it is found (for simulations in [4]-[6]) that even when vapor and liquid flows are unidirectional (or “one-way” or “parabolic”) due to local Peclet numbers (which appear in local discretization equations for the velocity components - see eqs. (5.61) – (5.64) in [20]) being very large (greater than 50,000 in both x and y directions for discretizations used in exit-condition sensitive simulation results reported here), the flows exhibit “elliptic” or “two-way” behavior leading to sensitivity to exit conditions. This *special* sensitivity to exit condition is due to “two-way” behavior of the vapor pressure fields (reflected, in the context of our computational methodology [4], by the “two-way” behavior of the pressure equations given by eqs. (6.30) – (6.31) in [20]) *combined* with the degree of freedom available with regard to relocation of the interface towards accommodating changed vapor flow fields through changed interfacial mass-fluxes. These equations for condensing flows are such that the coefficients that multiply the pressures at the locally upstream and downstream neighbors are comparable even for large Peclet numbers (see pressure discretization equations for SIMPLER procedure in Patankar [20]). Due to this, effects of changes in the exit pressure are felt by the entire vapor flow field which is then able to accommodate this change by changing the interface location and achieving a new flow field with different interfacial mass-transfer rates (and hence heat-transfer rates).

A much simpler support for the above result comes from simple one-dimensional modeling (leading to ordinary differential equations) of laminar/laminar internal condensing flows in a channel. It is appropriate to ignore the integral form of vapor momentum balance only for the gravity dominated external flow problem of Nusselt [21] and, occasionally, for some gravity driven channel flow analyses. For gravity driven internal (e.g. channel) flow analyses this approximation means condensate motion is not affected by vapor momentum balance because of negligible interfacial shear and freedom of the vapor to choose its exit pressure – which is a freedom that does not always exist. If one does not ignore the integral form of vapor momentum balance, the correct formulation of the problem is achieved (see, e.g., eqn. (53) of [22] for a horizontal channel). The ordinary differential equations for the correct formulation involves first order derivatives for other flow variables (interface speed $u_f(x)$ and film thickness $\delta(x)$ in [22]) but second order derivatives ($d^2\pi/dx^2$) of the variable $\pi(x)$ that represents the non-dimensional value of cross-sectional pressure. To solve this set of equations correctly, which was not done in [22], one needs exit pressure specification over and above specifications of inlet (pressure, velocity profile, and film thickness values) and wall temperature conditions. At the time of the analysis reported in [22], though eqn. (53) in the formulation given in [22] was correct, the solution was not. Instead of solving the equations for different exit pressures, the reported solution effectively chose only one exit pressure by an ad hoc mathematically specified value for the pressure gradient ($d\pi/dx$) at the inlet. In hindsight this was done to conform to the popular notion that the flow should be parabolic, even though the analytical formulation in [22] suggested that the flow is “elliptic” and requires exit pressure prescription. A serious problem with this type (as in [22]) of correct one dimensional steady formulation is that it *always* requires exit pressure specification as a boundary condition. Such an analysis is incapable of identifying the cases where exit pressure prescription is not required, such as fast partially condensing flows in ducts of small lengths or gravity driven steady flows in a vertical channel under unspecified exit conditions. In these cases, if the flow is allowed to choose its own exit pressure, it should self select its own “natural” exit pressure. The results based on unsteady solutions for these situations, which are presented here, exhibit presence of an “attracting” solution for the mathematically “ill posed” steady formulation. These results assure us that there exists a steady solution even in the

absence of exit pressure specification and the associated “ill-posed” steady formulation. There are other types of one-dimensional parabolic flow formulations/analyses that are frequently employed to allow turbulent vapor or wavy interface through introduction of an independently assumed model for “interfacial friction” S^i . This interfacial shear S^i relates to laminar liquid velocity profile through first equality in eqn. (A.7) of the Appendix but does not require satisfaction of the second equality in eqn. (A.7) of the Appendix – this is because vapor flow is allowed to be turbulent near the interface. The integral momentum balance for the vapor directly uses the interfacial friction S^i . Such steady formulations involve assumed “models” for interfacial shear S^i (see, e.g., Narain et al. [23]) and they work because the model functions are such that they can yield known values of S^i during forward marching of the solution through a first order system of non linear ordinary differential equations under prescribed initial conditions at the inlet. As shown later, with the help of the complete solution of the full two-dimensional steady/unsteady problems, results obtained from one dimensional theory employing such models can be good only over finite length problems involving partial condensation and sufficient vapor velocities (with either laminar or turbulent vapor flows). Therefore, these models are fundamentally flawed and need to be changed to allow second order derivatives in pressure (as is the case in [22]) if one is looking at complete condensation problems or sufficient downstream distances where vapor flows are slow and are sensitive to exit pressure.

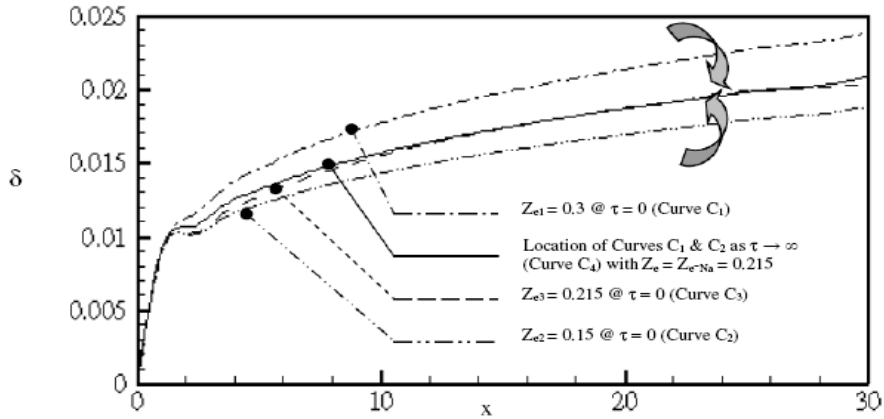


Fig. 2: For tube flow situations specified as in Phan et al. [6] (see their Table 1 and Fig. 2), the figure depicts three steady film thickness profiles (curves C_1 to C_3) for three different exit conditions for category I steady flows. The same figure is also used to show results for category II gravity driven flows once the exit condition specification is removed and the flow is allowed to seek its own exit condition (curve C_4). For category II flows, the figure indicates time trends for two sets of $\delta(x, \tau)$ predictions for $\tau > 0$. The curve C_1 starts at $Z_e = 0.3$ at $\tau = 0$, and, as $\tau \rightarrow \infty$, tends to the curve C_4 which represents the solution for $Z_e = Z_e|_{Na} = 0.215$. The curve C_2 starts at $Z_e = 0.15$ at $\tau = 0$ and tends, as $\tau \rightarrow \infty$, to the same curve C_4 . The curve C_3 represents category I solution when exit condition is held fixed exactly at the natural exit condition. As expected, the curves C_3 and C_4 overlap each other.

In the literature, condensing flows have been classified as to whether they are shear dominated or gravity dominated, internal or external, smooth or wavy at the interface, laminar or turbulent in the two phases, etc. It is proposed here that one can only make sense of the vast literature on forced internal

condensing duct flows if they are *also* classified in different categories based on the conditions imposed at the inlet *and* the exit. The following three categories (termed categories I – III) proposed here cover most cases of interest.

Category I (with complete or incomplete condensation under specified exit conditions)

- Prescribed or known values of total inlet vapor mass flow rate \dot{M}_{in} (kg/s), inlet vapor quality, inlet pressure p_{in} , and inlet temperature at all times t . Without loss of generality, one can focus on an all vapor flow (an inlet vapor quality of unity) at the inlet with known values of total inlet (all vapor) mass flow rate \dot{M}_{in} (kg/s), inlet pressure p_{in} , and inlet temperature (at saturation temperature $T_{sat}(p_{in})$ or at some superheat) at all times, t . This means the prescription could be steady or unsteady.
- Prescribed method of cooling that leads to known condensing surface (wall) temperatures $T_w(x,t) < T_{sat}(p_{in})$ for all x -locations over which film condensation occurs. Typical wall temperature conditions of interest are steady, but unsteady conditions are relevant to start-up and shutdown.
- Specified or known exit pressure conditions. For example, for steady exit conditions, exit pressure $p_e = \text{constant}$, which is equivalent, for steady partial condensation flow cases, to setting exit mass quality $Z_e \equiv \dot{M}_v \text{ (kg/s)} / \dot{M}_{in} \text{ (kg/s)}$ equal to an appropriate constant, where $\dot{M}_v \text{ (kg/s)}$ is the vapor mass flow rate at the exit.

For category I partial condensation flows with steady specified exit pressure and other conditions, the computational simulation results shown in Fig. 2 are the solutions of the formulation given here in the Appendix. The flow conditions and formulation are the same as the ones specified for Fig. 2 and Table 1 of Phan et al. [6]. The results show three different steady solutions (curves C_1 to C_3) for three different specified vapor qualities Z_e at the exit (viz. $Z_{e1} = 0.3$, $Z_{e2} = 0.15$ and $Z_{e3} = 0.215$). Some of the Garimella et al. experimental investigations ([24]-[25]) are for flows in this category with inlet quality $Z_i (< 1)$ and exit quality Z_e specified at values incrementally smaller than Z_i .

Category II (with complete or incomplete condensation under unspecified exit conditions)

- Prescribed or known values of inlet mass flow rate \dot{M}_{in} (kg/s), inlet pressure p_{in} , and inlet temperature (at saturation temperature $T_{sat}(p_{in})$ or at some superheat) at all times, t . Without loss of generality, it is assumed that the flow is all vapor at the inlet.
- Prescribed method of cooling leading to known wall temperatures $T_w(x,t) < T_{sat}(p_{in})$ for all x -locations over which film condensation occurs.
- Exit condition is not specified. However, due to some system hardware limitations and constraints, if only a range of exit conditions (i.e. pressures) is available and the condenser is freely able to choose its “natural” exit pressure within this range, we still call it a category II flow. On the other hand, in the case of the availability of only a limited range of exit pressures, if the flow *seeks* a “natural” value that is at or outside the boundary of the limited range, the flow is *not* considered a category II flow.

For category II unsteady partial condensation flows with unspecified exit pressure or exit quality, the computational simulation results shown in Fig. 2 are the solutions of the formulation given here in the Appendix. The steady formulation for this problem is however “ill-posed.” The flow conditions and formulation are the same as the ones specified for Fig. 2 and Table 1 of Phan et al. [6]. For these gravity driven condensate cases of category II flows shown in Fig. 2, it is computationally shown that if exit vapor quality specification constraints at $Z_{e1} = 0.3$ or $Z_{e2} = 0.15$ are removed at some time ($\tau = 0$) – and subsequently ($\tau > 0$) one does not specify any exit condition in the unsteady mathematical model (which is equivalent to not specifying exit pressures and allowing them to vary over a certain range), the solutions show that the experimental flow in this category should be able to select, in accord with the predictions, a quasi-steady flow with a “natural” value of exit quality (curve C₄, representing $Z_{e3} = Z_{e-Na} = 0.215$). However, as discussed later, experimental arrangements for category II flows require special design and the available range of experimental conditions may not include the “natural” exit condition the flow is seeking. It is also possible that natural “attractors” for category II flows are weak or do not exist, as is shown to be the case for some horizontal and zero gravity condensing flows discussed later. For these cases, the concave bowl analogy schematic for “attractors” given in Fig. 9 of Narain et al. [4] needs to be replaced by a flat or weakly concave shape for this bowl. Therefore, the existence of steady solutions is at the mercy of other factors such as whether or not an “attracting” steady solution exists and, if it does, whether or not downstream conditions in the experimental set up are conducive to the attainment of this “attracting” solution and associated exit condition.

As a matter of semantics, it should be noted that, for category II flows, in Phan et al. [6], existence of an “attractor” leading to a long-term steady exit condition was termed differently – it was called a long-term “one-way” or “parabolic” behavior. Similarly, non-existence of an “attractor” (typically an indicator of flows that lie outside the annular regime and are more complex in the sense that they exhibit certain degrees of randomness or indeterminacy) was termed differently in [6] – it was called long-term “two-way” or “elliptic” behavior.

Category III (Complete condensation involving special specified conditions

at the inlet and the exit)

Though, technically, this is a special subcategory of a general unsteady and/or steady category I flows, it is listed separately because it typically involves and often used specialized experimental set-up and hardware facilities. This class of condensing flows has been extensively investigated in the experimental literature ([12]-[19]) for steady or oscillatory flows.

- In this case there is a constant pressure reservoir, with a stagnation pressure $p_{\text{Tank-in}}$, that feeds the vapor flow (at inlet mass flow rate $\dot{M}_{\text{in}}(t)$, pressure p_{in} , temperature $T_{\text{V-in}}$, and density $\rho_{\text{V-in}}$) into the test section through an inlet valve (with valve coefficient k_i). This requires the inlet pressure, p_{in} , to satisfy at any time t :

$$p_{\text{in}} \cong p_{\text{Tank-in}} - k_i \frac{\dot{M}_{\text{in}}(t)^2}{\rho_{\text{V-in}}} \quad (1)$$

- Also, there is a constant pressure exit tank, with a stagnation pressure $p_{\text{Tank-exit}}$, to which the condensate flows through an exit valve of valve coefficient k_e . The exit valve handles an *all liquid* flow because this case is only for complete condensation flows. At the exit of the condenser, the

liquid flow rate is \dot{M}_{exit} at any time, t , and the liquid density is $\rho_{L\text{-exit}}$. This requires that the test section exit pressure, p_{exit} , satisfy at any time t :

$$p_{\text{exit}} \cong p_{\text{Tank-exit}} + k_e \frac{\dot{M}_{\text{exit}}(t)^2}{\rho_{L\text{-exit}}} \quad (2)$$

- Prescribed or known *steady* wall temperatures $T_w(x) < T_{\text{sat}}(p_{\text{in}})$ for all x -locations over which film condensation occurs.

The experimental and/or modeling analysis papers of Wedekind et al. ([12], [15]), Bhatt et al. ([13]-[14], [16]), Kobus et al. ([19]), Liao et al. ([26], [27]), etc. focus on category III flows for a horizontal condenser. Our theory and experiments also suggest what they find, namely, unless $p_{\text{Tank-in}}$ and $p_{\text{Tank-exit}}$ are sufficiently compatible with system parameters (valve coefficients k_i and k_e) for a desired steady value of \dot{M}_{in} , an oscillatory flow may result with unsteady and oscillatory inlet and exit pressures (viz. p_{in} and p_{exit}).

The experiments and computations in this paper, however, focus only on steady category I and category II partial condensation flows. As a result, the flow transients and system instabilities reported in this paper, as far as flows within the test-section are concerned, are necessarily of different origin. However, at a system level, the experimentally observed flow oscillations' relationship to the better known ([14], [16]) results for category III flows in the downstream auxiliary condenser is also discussed here.

The experimental runs reported here largely involve laminar condensate and turbulent vapor situations with possible vapor compressibility effects for some of the category I flows. Despite this, both qualitative and quantitative comparisons with simulation results based on the laminar-vapor/laminar-condensate methodology given in [4]-[6] are possible for a feasible subset (within the boundaries for steady annular flows) of experimental runs. This comparison is presented here and is possible because turbulent vapor often laminarizes in the vicinity of laminar condensate as the condensate is slow and remains laminar approximately up to $Re_\delta \leq 1800$ (see film Reynolds number, Re_δ , defined in Phan and Narain [28]). Also, for gravity driven condensate cases considered here, the existence of turbulent vapor zones in the core and entrance zone of the condenser has only minor second order impact on most of the flow variables with first order effects limited to pressure variations in the condenser. The far field vapor turbulence often tends not to be a significant player because the overall flow features (local and average heat transfer coefficients) are dominated by interfacial mass and heat transfer rates, which are governed by the typically laminar nature of the gravity driven condensate flow and the associated laminar nature of vapor flow in the vicinity of the interface. Because of the above, all experimental runs reported here for partial (or incomplete) condensation cases involving laminar condensate show a very good *qualitative* agreement with the simulations as far as the existence of multiple steady solutions for multiple steady exit conditions (category I) and a "natural" steady solution for the unspecified exit condition cases (category II) are concerned. The agreement with simulations, with regard to exit vapor quality and general consistency with overall heat transfer rates, are also *quantitatively* very good for category II experimental runs that fit the annular flow assumption for the simulations.

The experiments reported here involve a single pure working fluid (viz. FC-72 by 3M Corp.) and focus on inlet mass flow rates that correspond to inlet vapor Reynolds numbers in the range of 10,000 - 40,000 and vapor to wall temperature differences of 3 - 60°C (i.e. $0 \leq Ja \leq 0.4$).

Furthermore, computational results for external condensing flows that are obtained from this simulation tool have proven record (see Phan and Narain [28] and Kulkarni et al. [2]–[3]) of making qualitatively and quantitatively correct predictions for steady flows. The steady flow predictions are in excellent agreement with the classical solutions of Nusselt [21] and Koh [29]. Additionally, the unsteady results obtained from this computational tool are also able to accurately predict wave phenomena and their effects for these benchmark classical problems.

Hitherto nonexistent accounting of exit condition categories (and exit condition parameter “ ϕ ” introduced later in this paper for internal condensing flows, as discussed in section 6), is perhaps one of the reasons for the large uncertainties and deficiencies noted by Palen et al. [30] with regard to the poor usefulness of quantitative information available from existing correlations for heat transfer coefficients.

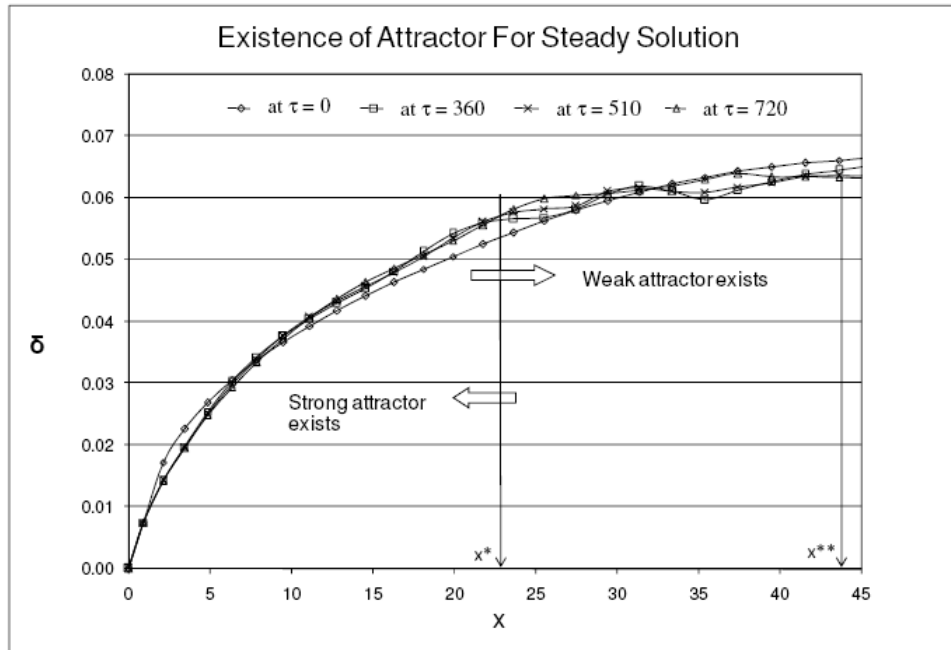


Fig. 3: For a channel ($h = 0.004$ m) in $0g$ environment and flow of R113 at uniform inlet speed $U = 0.6$ m/s and temperature difference $\overline{\Delta T} = 5^\circ\text{C}$, the figure shows non-dimensional film thickness at different non-dimensional times (see [6]). A zone with strong steady attractor is seen in the initial part of the channel and the zone after $x^* > 23$ exhibits weak unsteady attraction to a quasi-steady solution.

Instead of the strongly attracting solutions for gravity driven category II flows in a vertical channel (of the type shown in Fig. 2), one obtains significantly weaker attracting solution for horizontal channel or $0g$ channel flow situations and this is exemplified by Fig. 3 where an attractor exists only for $0 \leq x \leq x^* \approx 23$ with the attractor’s strength diminishing with increasing distance from the inlet. For $x^* \leq x \leq x^{**} \approx 45$ in Fig. 3, the “attractor” can be seen to have morphed into a rough “attracting zone” that is sufficiently weak and wavy and thickens with increasing x (no initial disturbance were imposed – the simulations are showing amplified computational disturbances). For $x \gg x^{**} \approx 45$ locations that are not shown in Fig. 3, the “attracting zone” is non-existent and true “elliptic” nature of the problem manifests

itself for unspecified exit condition category II flows - making the flow physically and computationally indeterminate. Furthermore, it is found that x^* increases/decreases with increasing/decreasing inlet mass flow rate (per unit depth of the channel) $\dot{M}_{in} = \rho_2 U h$ and, for $x^* \rightarrow 0$, there is a positive non-zero lower threshold of mass flow rate – termed \dot{M}_{in-cr} - for which no steady flow exists over any length of the channel. Therefore, if the category II flow is one of partial condensation and the length of the channel is x_e , then we have the following possibilities: the flow has an “attractor” if $x_e < x^*$, it has a weak “attractor” over $x^* \leq x_e \leq x^{**}$ if x_e is in this range, and the flow has no solution possible under category II conditions if $x_e \gg x^{**}$. In other words, fully condensing steady flows of this type (stratified/annular) in micro-gravity or horizontal channel is an impossibility for category II flows. However, as shown later, a fully condensing steady flow under category I or III flow conditions with suitably prescribed inlet pressure, exit pressure, and cooling method (i.e. condensing surface temperature $T_w(x)$) is possible and can be arranged (this allows for non-annular plug-slug flow regime near the point of full condensation) for zero gravity or shear driven horizontal situations. If the exit pressure chosen for realization of category I flow is not compatible with inlet and other conditions, oscillatory flow may result.

The above results also make physical sense. The attractor for gravity driven cases under category II flows arise because of the irrelevance of vapor motion as the condensate is driven by gravity and the vapor motion is eventually (near the point of complete condensation) determined by a liquid flow which is allowed to flow and get whatever pressure it seeks. However since the entire flow morphology can easily be changed by a “non-natural” externally imposed prescription of exit-pressure under category I conditions, the category II attainment remains sensitive. For shear driven horizontal or micro-gravity flows, existence of an annular/stratified “attractor” of the type being sought here requires sufficiently fast vapor flows $\dot{M}_{in} > \dot{M}_{in-cr}$ that can provide sufficient shear and determine pressure fields over a certain length x^* of the duct. However, the definition/existence of this attractor is in jeopardy if the vapor motion is not sufficiently well defined; this which happens, for unspecified exit pressures, after a certain distance x^* .

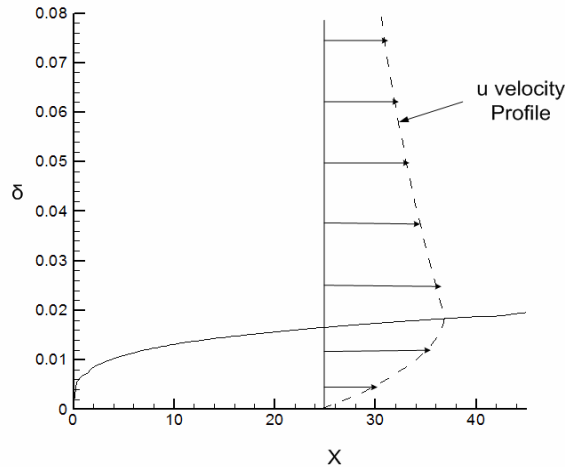


Fig. 4a: The figure shows the non-dimensional film thickness and the u versus y velocity profile (at $x = 25$) for steady solution of the typical Nusselt problem (see [28]) with $\overline{\Delta T} = 5^\circ\text{C}$.

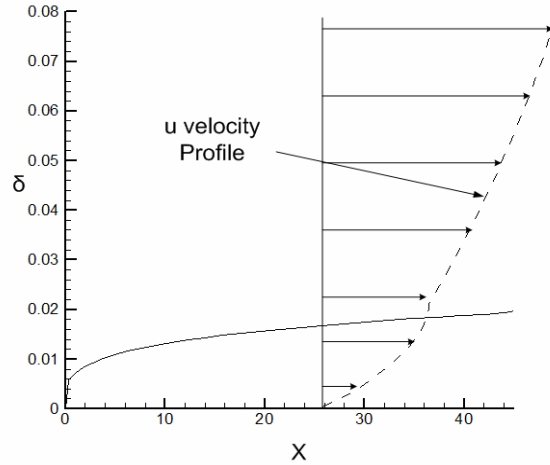


Fig. 4b: For a forced flow with $U = 0.2$ m/s and all other conditions remaining the same as in Fig. 4a, this figure shows the non-dimensional film thickness and the u velocity profile (at $x = 25$) obtained from a steady solution of the problem. It can be seen that the film thickness values do not change, as compared to the those in Fig. 4a, but u velocity profiles and associated shear values are different for the two cases.

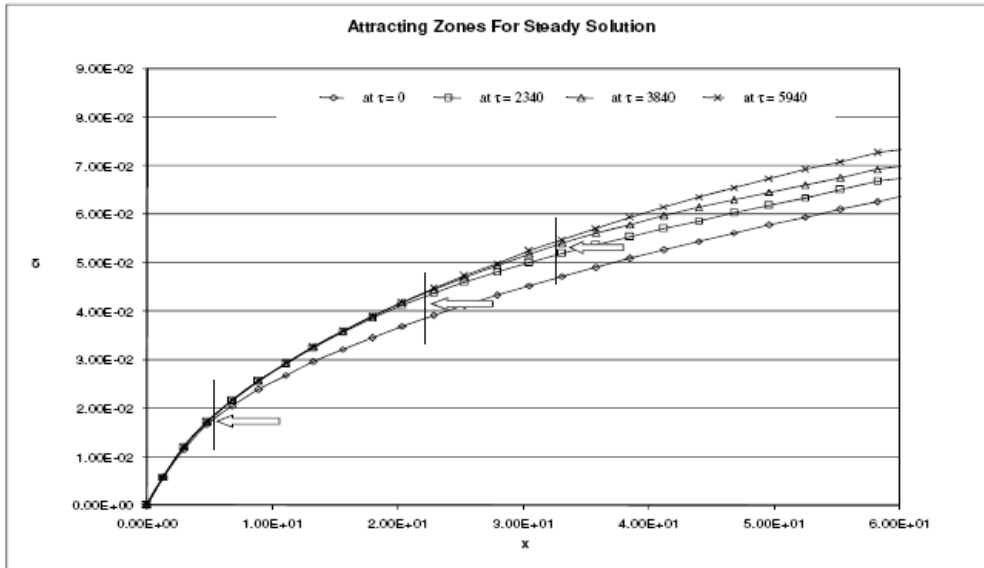


Fig. 5: For a horizontal condensing flow over a flat plate (see [3]) with $U = 1.7$ m/s and $\overline{\Delta T} = 5^\circ\text{C}$, this figure shows non-dimensional film thickness at different non-dimensional times given by the unsteady solution of the problem. An initial guess given at time $\tau = 0$ is seen to get attracted to the long term steady solution at different rates. This rate decreases along the length of the plate. The markings demarcate the zones that converged into steady solution at different times.

In fact the strong versus weak attractor situations depicted, respectively, in Figs. 2 and 3 for vertical and 0g channel flows is quite typical and are also present, respectively, for their external flow counterparts, namely the Nusselt problem (see [28]) and the Koh problem (see [2]-[3]) as well. Note, however, both the Nusselt [21] and the Koh [29] problems have well defined uniform pressure values at the inlet, far field, and at the finite exit location used to model the infinite plate. Therefore, in a sense, the solution of these problems, particularly the Koh problem [29] for which vapor motion is important, should behave more like a category I than a category II flow problem. The steady solution shown in Figs. 4a and 4b are for Nusselt problem and Nusselt problem in the presence of forced convection respectively. The depicted steady interface locations shown in Figs. 4a and 4b are strong “attractors” as they have also been obtained, though not shown here, in the limit of $\tau \rightarrow \infty$ solutions of the unsteady problem with an initial condition different than the long term steady solution itself. As seen from the comparison of Figs. 4a and 4b, for the case considered, the film thickness does not change in the presence of forced convection as the vapor motion remains unimportant. This is because, for both cases, gravity is the dominant force in driving the condensate and the steady solutions shown and generally obtained (see [28]) satisfy the well known analytical results (see [21] and [28]) for film thickness in the presence or absence of waves. In comparison, the representative 0g solutions (obtained by solving the unsteady equations in [2] – [3] for the Koh problem [29]) shown in Fig. 5 are possible only if U is above a certain lower threshold (termed $U_{\infty|L-cr}$ in [3]). Furthermore the solution in Fig. 5 exhibits the presence of an “attractor” whose attracting strength decreases with increasing x . The existence of a threshold inlet speed is similar to what is needed for the channel flow in Fig. 3 – but the Koh problem [29], being a category I external flow problem has an “attractor” which theoretically exists at all x locations (i.e. there is no x^* as in Fig. 3). Despite this, in Kulkarni et al. [2]-[3], it is shown that the weak attractor at downstream locations becomes more noise-sensitive and amplifies ever-present minuscule noise (condensing surface vibrations, etc.) leading to persistent and large amplitude waves around $Re_x|_{wavy-cr} \approx 5 \times 10^5$. Further downstream of this, the condensate is expected to become turbulent.

2. EXPERIMENTAL FACILITY

The condenser section, which is of the type shown in Figure 1a, is typically a *part* of a closed flow loop. The flow loop, which maintains a steady inlet pressure (p_{in}) and mass flow rate (\dot{M}_{in}) at the inlet, while maintaining a prescribed steady (and nearly uniform) condensing surface temperature, may be designed to provide different categories of exit conditions. Exit condition specifications for category I and category II partial condensing flows defined earlier in section 1 are realized through flow arrangements indicated in Fig. 6 and Fig. 7 respectively.

A 0-500 W evaporator/boiler in Figs. 6-7 is used to evaporate the working fluid (FC-72). The vapor mass flow rate out of the evaporator, \dot{M}_v , is fed into the test section. This mass flow rate is measured by a Coriolis flow meter F_1 and, during transients, this value can be controlled by the pneumatically actuated control-valve V_1 (shown connected to F_1 in Figs. 6-7). Under steady conditions though, the value of \dot{M}_v gets approximately fixed by the net steady electrical heating rate for the evaporator. This is due to the restriction imposed by the evaporator energy balance, viz., $\dot{M}_v \approx \dot{Q}_B / h_{fg}(p_B)$. Here \dot{Q}_B is the net heat rate into the evaporator, p_B is the steady evaporator pressure, $T_B \approx T_{sat}(p_B)$ is the steady evaporator temperature (which is nearly equal to the saturation temperature of the fluid at pressure p_B), and h_{fg} is the heat of vaporization at the liquid/vapor surface pressure p_B in the evaporator. Towards reduction in start-up time to steady state in the evaporator, the liquid flowing in the evaporator is warmed up,

(between points P' and B' in Figs. 6 – 7) so its temperature is nearly equal to the evaporator temperature $T_B \approx T_{\text{sat}}(p_B)$.

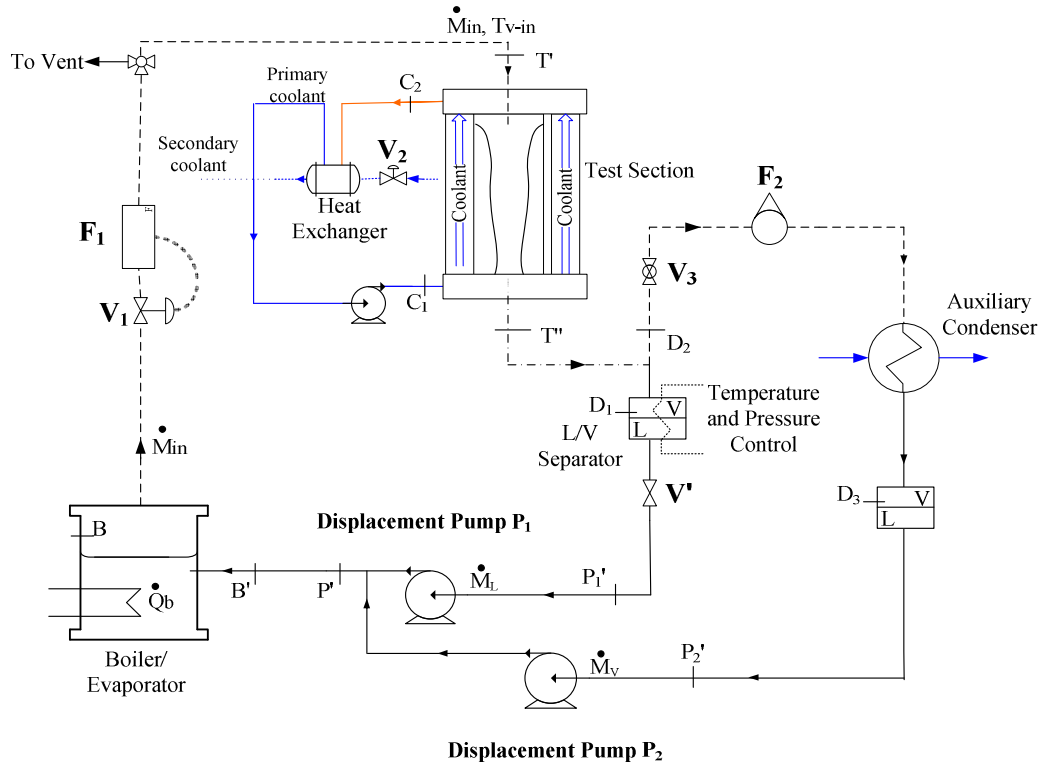


Fig. 6: The schematic of the flow loop for achieving specified exit condition category I flows for partial condensation cases.

The test-section is a 0.8 m long, vertical, stainless steel (316 SS) tube with 6.6 mm inner diameter, D , and 12.7 mm outer diameter. At the entrance of the test-section, the inlet vapor temperature is denoted as T_{V-in} , the inlet pressure is denoted as p_{in} , and the inlet vapor is kept slightly superheated (2-10°C superheat obtained by heating a relevant portion of connecting tubes by a rope heater). A suitable thermocouple and an absolute pressure transducer respectively measure the temperature, T_{V-in} , and pressure, p_{in} , of the vapor at the inlet. The dynamic view from an axial boroscope, mounted at the top of the test-section shown in Fig. 8, is used to visualize and ascertain the nature of the flow in the first half of the test-section. However, because of sharpness and contrast improvements that are needed for better quality images, snapshots and video clips of the flows are not included in this paper. They are, however, expected to be available in the near future. We are currently able to use these views to ascertain whether or not annular film condensation begins near the indicated “start of condensation” point in Fig. 8 and, also, to ascertain (and then to ensure) dryness of the vapor up to the test-section inlet.

The test-section (see Fig. 8) is suitably instrumented with various sensors (thermocouples, pressure transducers, etc.). For future work, it will be possible to obtain local film thickness data through integration of our recently invented, non-intrusive film thickness sensors that utilize the principle of fluorescence and fiber-optic technology (see Ng [31]) and are able to measure the “local” time-varying

thickness of dynamic liquid films. The technique used for mounting all the sensors in Fig. 8 is described in detail in [32] - [34].

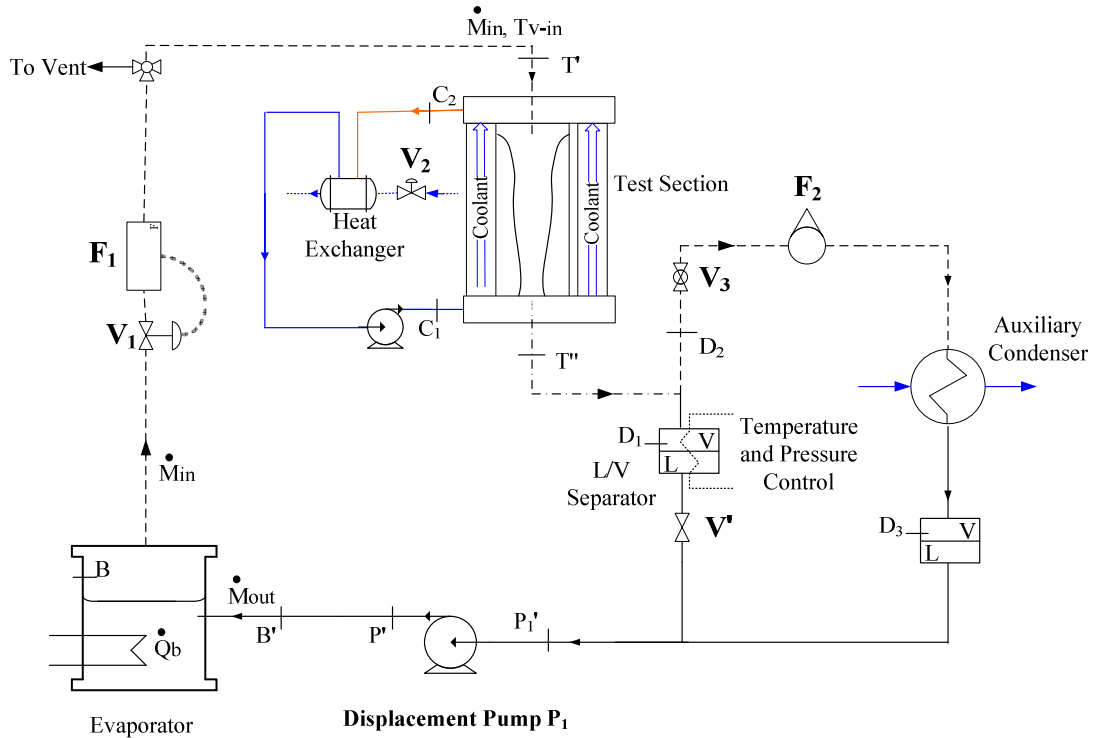


Fig. 7: The schematic of the flow loop for achieving unspecified exit condition category II flows for partial or full condensation cases.

The test-section in Fig. 8b (not shown to size relative to the outer tube in Fig. 8a) is centrally aligned in the hollow space of a larger diameter stainless steel (314 SS) tube. This outer tube has an inner diameter of 23.62 mm and an outer diameter of 25.40 mm. The test-section tube is cooled by the flow of cold water in the annulus formed by the outer surface of the test-section tube and the inner surface of the outer tube. As shown in Figs. 6-7, the flow of coolant water is arranged by a separate closed loop consisting of the shell-side of the shell-in-tube heat exchanger (flow is on shell-side) and a pump. A separate loop, not shown in Figs. 6-7, assures secondary coolant (cooler-water) flow at a steady constant temperature and a steady flow rate through the tube-side of the heat exchanger in Figs. 6-7. This loop (see Kurita [33]) replaces the open drain water loop used in the preliminary experiments. This loop has two chillers in series (one for coarse and one for finer control of temperature) and this provides for a good control of the steady value of temperature T_{C-in} (marked in Fig. 8a) at the coolant inlet location in Figs. 6-7. This, in turn, enables repetition of experimental runs regardless of seasonal variations in drain water temperature.

Resistance temperature detectors (RTDs) and type-T thermocouples measure temperatures at different locations of the test-section (see Fig. 8) and at other flow loop locations marked by points B, B', T', C₁, C₂, D₁, D₂, P'₁, P'₂, and P' in Figs. 6-7. A barometer measures outside atmospheric pressure.

Flow meters at locations marked F_1 (Coriolis meter that directly measures mass flow rate), F_2 (a volume flow rate measuring rotameter), P_1 (volume flow rate meter imbedded in pump P_1), and P_2 (volume flow rate meter imbedded in pump P_2) yield mass flow rates through those locations. Absolute pressure transducers measure pressures at test-section inlet (location 1 in Fig. 8), and at locations B and D_2 in Figs. 6 - 7. Differential pressure transducers measure pressure differences in the test-section (in Fig. 8a, this is between locations 1 and 9, location 3 and outside atmosphere, and location 6 and outside atmosphere). Two electronically controllable displacement pumps P_1 and P_2 (see Figs. 6-7) can pump liquid FC-72 at a steady or unsteady specification of volume or mass flow rates. A pneumatically controlled valve V_1 is used, as needed, to control mass flow rate through F_1 . Most of the details of the employed data acquisition system are explained in Narain et al. [34] and Siemionko [32].

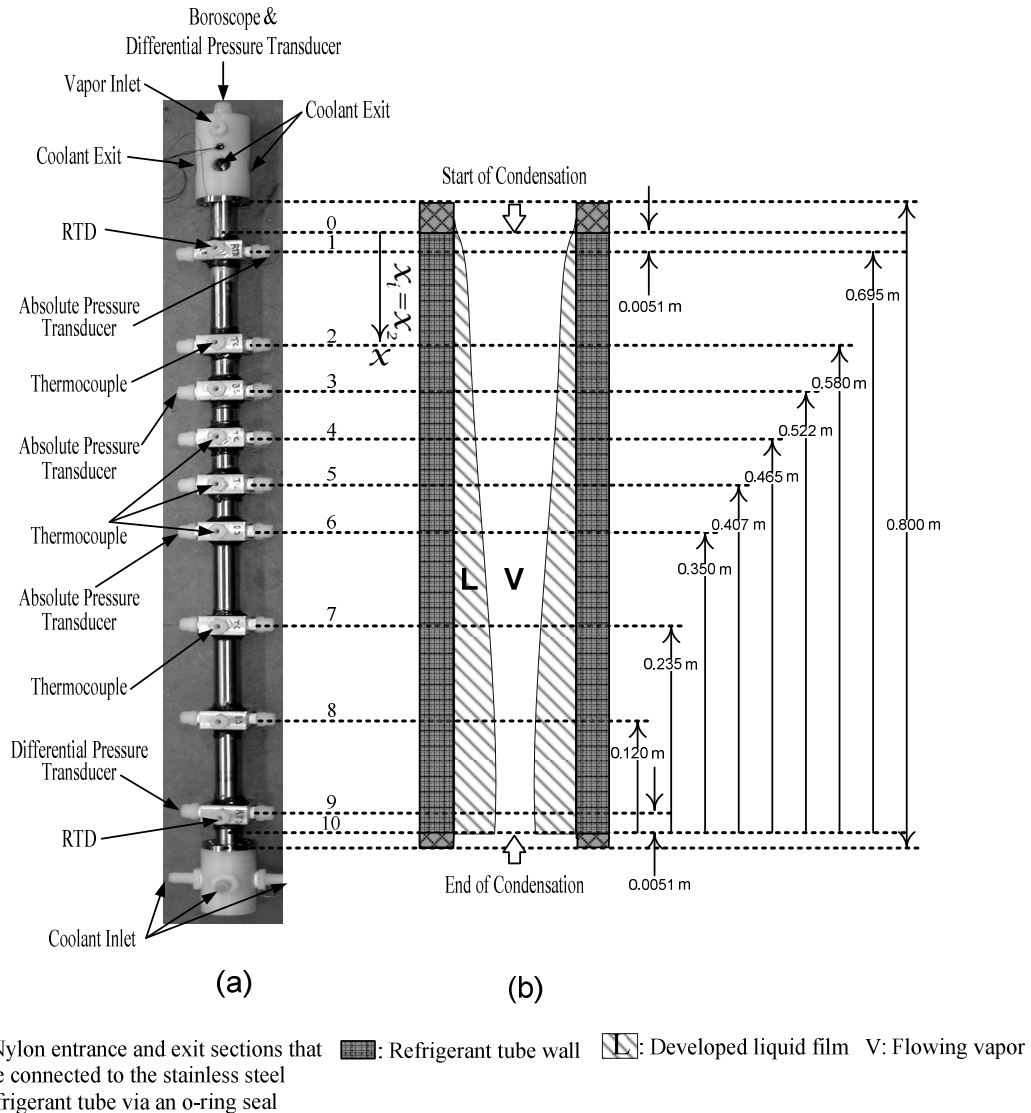


Fig. 8: (a) The photograph of condenser test-section. (b) The test-section schematic (diameters in (a) and (b) are not to the same scale). The condensing surface covers the zone $x_0 \leq x \leq x_{10}$.

For convenience, the system in Figs. 6-7 is broken into the following sub-systems. (i) Sub-system \mathcal{A} is the portion of the flow loop between points P' and T' (this portion contains the flow into the evaporator, the evaporator, the flow meter F_1 , valve V_1 , and the tubing leading the flow into the test-section). (ii) Sub-system \mathcal{B} is the portion of the flow loop between points T' and T'' (this portion consists of the test-section). (iii) Sub-system \mathcal{C} is the portion of the flow loop between points T'' and P' (this portion consists of the L/V separator, the two branches of the flow in the liquid line and the auxiliary-condenser line, and the pump or pumps). (iv) Sub-system \mathcal{D} is the portion that consists of the primary coolant loop shown in Figs. 6-7 and a secondary coolant loop (not shown here but shown in Kurita [33]). The sub-systems \mathcal{A} - \mathcal{D} defined above are not marked in Figs. 6-7 but the definitions introduced here are necessary for later discussions of the experimental results.

Additional details of this experimental facility (rather of a similar earlier version), data-acquisition, and LabView 7.1 based data processing and instrument control strategies are available in Siemionko [32].

3. EXPERIMENTAL PROCEDURE

Here we describe the procedure for investigating partial condensation cases under different exit conditions. Some procedure and results for fully condensing cases are also given in Narain et al. [1]. Note that results from different exit conditions are to be compared for approximately the same inlet mass flow rate \dot{M}_{in} , inlet pressure p_{in} , and temperature difference $\overline{\Delta T} = T_{sat}(p_{in}) - \overline{T}_w$, where \overline{T}_w is the mean condensing surface temperature. Pure vapor may be allowed to enter the test section with a superheat of 2-10°C. The purging process (see [32]) ensures that the vapor flowing in the test section is pure over the duration of the experimental run and that non-condensable air in the flow loop has zero to insignificant presence. Note that vapor Jakob numbers $Ja_V (\equiv C_{p2} \cdot \Delta T_{sup} / h_{fg}(p_{in}))$, where C_{p2} is the specific heat of the vapor and $h_{fg}(p_{in})$ is the heat of vaporization at pressure p_{in}) represent the ratio of sensible cooling of vapor to heat of vaporization. Since these numbers are very small ($< 1.0 \cdot 10^{-5}$) in comparison to liquid Jakob numbers $Ja (\equiv C_{p1} \cdot \overline{\Delta T} / h_{fg}(p_{in}))$, where C_{p1} is the specific heat of the liquid condensate), vapor temperature can be effectively modeled as a steady constant equal to the inlet saturation temperature. The steadiness of \dot{M}_{in} primarily depends on the constancy of heat supply to the evaporator (which is easily achieved by constant electric heating at a known wattage) and the eventual approximate steadiness of the evaporator pressure p_B . Even if the steady value of p_B changes somewhat for different start-ups, as long as the corresponding evaporator saturation temperature $T_B = T_{sat}(p_B)$ changes negligibly, it is found that the remaining flow loop pressures relative to a single effective boiler pressure are the same for two independent repetitions of the same experimental run (i.e. same \dot{M}_{in} , $\overline{\Delta T}$, \overline{T}_w , and Z_c). This is true because all other pressures, p , are effectively characterized by their pressure differences, $p - p_B$, relative to this pressure p_B . Alternatively, a previously obtained steady value of p_B can be regained by bringing the new evaporator pressure back to roughly this same value by: (i) use of a newly developed electronically controlled accumulator discussed in section-6, or (ii) by suitably switching the heater on and off under same steady heating rate, or (iii) by gradually venting the evaporator from a higher pressure to the desired earlier value of p_B . The last two of the above described processes have been used to successfully assess the repeatability of a few representative experimental runs. With regard to constancy of water temperature T_{C-in} at the coolant inlet for the test-section (see Fig. 8) over time; achieving constancy of water temperature and its flow rate in the secondary coolant loop (not shown here) proved to be sufficient.

Specified Exit Conditions (Category I flows)

Incomplete or partial condensation flows

For investigation of specified conditions (through a steady and specified exit vapor quality) at the exit that involve partial condensation flows through the test-section, the arrangement in Fig. 6 is used. In this arrangement, the liquid at the exit flows out of the test-section at a mass rate of \dot{M}_L , goes through the liquid/vapor (L/V) separator, and is pumped by pump P₁ back into the evaporator. Both the pumps P₁ and P₂ (displacement pumps made by Masterflex) in Fig. 6 allow digital control of flow rates. The vapor at the exit flows out of the test-section at a mass flow rate of \dot{M}_V and is measured through a volume and mass flow rate measuring rotameter F₂. This vapor then flows through an auxiliary condenser where the vapor is completely condensed into liquid, goes through the pump P₂, and then, on its way to the evaporator, merges near point P' (see Fig. 6) with the liquid flowing out of pump P₁.

The control strategy, to achieve a specified steady flow with a prescribed exit vapor quality ($\dot{M}_V/\dot{M}_m \equiv Z_e$) for a given inlet and wall conditions, is to initially hold valve V₁ open at a fixed level of opening while ensuring (as described in the first paragraph of this section) desired steady values of \dot{M}_m , p_B, and $\overline{\Delta T}$. Then the exit vapor mass rate \dot{M}_V through pump P₂ (or rotameter F₂) is held fixed at a value less than the inlet mass rate \dot{M}_m while exit liquid mass flow rate \dot{M}_L is varied through pump P₁ at a value given by the tracking equation: $\dot{M}_L|_{P_1} = \dot{M}_m - \dot{M}_V|_{\text{Rotameter}}$.

As the flow through the evaporator becomes steady, \dot{M}_m becomes steady, and, at that time, we may or may not need to hold this value actively fixed with the help of controllable valve V₁. At this stage, active control of valve V₁ does not achieve much except that it eliminates some unwanted minuscule drifts in the inlet mass rates. For a given set of inlet (\dot{M}_m , p_{in}, T_{V-in}) and wall (\overline{T}_w) conditions, different specified steady states are achieved by the above strategy for different values of \dot{M}_L . Examples of experimentally achieved partial condensation flows under specified exit conditions (category I flows) are given and discussed in the next section.

Unspecified Exit Condition Cases (Category II flows)

“Natural” Partial Condensation

For obtaining/investigating existence of a “long term,” steady, “natural” exit condition for category II flows (under unspecified exit conditions) with all other conditions being kept the same as in a corresponding specified exit condition case in category I, the flow is required to go through the test-section and onwards under the arrangement shown in Fig. 7. Note that this arrangement has a single displacement pump as opposed to the two displacement pumps used in the arrangement of Fig. 6. The approach is to hold values of \dot{M}_m , p_B, and $\overline{\Delta T}$ nearly the same as in one of the specified category I cases while the pump P₁ in Fig. 7 is *controlled* such that the mass flow rate through it tracks the equation: $\dot{M}_L|_{P_1} = \dot{M}_m$. If start-up and other conditions (such as the range of pressures allowed in the L/V separator) allow a steady state flow, with gravity driven condensate, is attained in which, at the exit of the test-section, the inlet vapor mass flow rate is split, by a natural selection process, into a liquid condensate flow rate $\dot{M}_L|_{N_a}$ and a vapor flow rate $\dot{M}_V|_{N_a}$. Clearly these values satisfy the equation: $\dot{M}_m = \dot{M}_L|_{N_a} + \dot{M}_V|_{N_a}$. Examples of experimentally achieved partial condensation flows under unspecified exit conditions (Category II flows) are given and discussed in the next section.

4. EXPERIMENTAL RESULTS, DISCUSSIONS, AND COMPARISONS WITH SIMULATIONS

The column headers in Tables 1-2 indicate accuracies of the values of key *measured* variables obtained through flow loops' instruments and sensors. Overall accuracy bounds for the reported *calculated* variables (such as \bar{q}'' , \bar{h} , etc.) are also shown. The non-dimensional numbers Re_{in} , $x_e = L/D = 106$, Ja , ρ_2/ρ_1 , and μ_2/μ_1 in Tables 1-2 define the flows and they are defined in [4]-[6]. In Tables 1-2, the heat flow rate \dot{Q}_{out} and associated average heat transfer coefficients (\bar{h}) are obtained through the relation: $\dot{Q}_{out} \approx \dot{M}_L h_{fg} = \bar{h}(\pi DL) \overline{\Delta T}$. The inlet vapor mass-flux G in Tables 1-2 is defined as $4\dot{M}_{in} / (\pi \cdot D^2)$.

All (except the Coriolis meter F_1) of the instruments' accuracies for *measured* variables were established after their in-house calibrations with the help of suitable and reliable reference instruments of known resolution and appropriate reference physical conditions (temperature, flow rate, pressure, etc.). The accuracy of the Coriolis meter was established by the vendor support staff at the time of its installation. The error estimates for the *calculated* variables reported in Tables 1-2 were obtained by well-known standard procedures (see, e.g., eqs. (3.27)-(3.28) in Parratt [35]). The accuracies of individual *calculated* variables in a column were taken into account to report maximum values of the errors in the column headers of Tables 1-2. All the individual values of errors were either less than or equal to these reported error values. The error definitions, associated error analyses and calibration accuracies can be found in Narain et al. [34].

Table 1: Experimentally measured data and some key calculated and computed variables for steady states achieved for category II (unspecified exit condition) partial condensation flows.

Run No.	\dot{M}_{in}	\dot{M}_V	Z_c	Z_c	\bar{T}_W	T_{sat}	$\overline{\Delta T}$	p_{in}	p_{x6}	p_{T^*}	Δp	p_{D2}	ρ_2/ρ_1	μ_2/μ_1	G	Re	Ja	Pr_1	\dot{Q}_{out}	\bar{q}''	\bar{h}
	(g/s)	(g/s)	EXP	COMP	(K)	(K)	(K)	(kPa)	(kPa)	(kPa)	(kPa)	(kPa)			(kg/m ² s)				(J/s)	(W/m ²)	(W/m ² K)
	±0.05	±0.04	±0.04		±1	±0.15	±1	±0.6	±0.6	±0.7	±0.05	±2	±0.0001	±0.0001	±1.5	±900	±0.02	±0.02	±5	±800	±80
1	1.44	0.48	0.33	0.33	320	331.49	11	107.3	109.3	106.5	-0.82	105	0.0085	0.0243	42.1	23900	0.14	9.61	81	5200	453
2	1.76	1.08	0.62	0.57	317	325.23	8	87.0	86.4	88.0	-0.36	85	0.0070	0.0223	51.5	29700	0.10	10.11	58	3700	450
3	1.54	0.69	0.44	0.36	323	335.55	12	122.6	116.6	116.1	-0.19	114	0.0097	0.0260	45.0	25300	0.15	9.21	71	4500	387
4	1.29	0.49	0.38	0.38	320	329.64	10	101.0	102.4	100.8	-2.09	98	0.0081	0.0230	37.7	21500	0.11	9.69	68	4300	476
5	1.70	0.83	0.51	0.52	324	332.55	9	111.0	112.5	111.0	-0.93	109	0.0089	0.0252	49.6	28100	0.11	9.37	70	4400	508
6	1.17	0.47	0.40	0.39	320	332.64	13	111.3	NA	111.3	-0.12	109	0.0088	0.0246	34.2	19325	0.16	9.55	59	3700	298
7	1.31	0.49	0.37	0.37	321	330.85	10	105.0	106.8	104.5	-2.06	102	0.0084	0.0244	38.3	21700	0.12	9.58	69	4400	462
8*	1.93	1.39	0.72	0.72	322	325.55	4	84.6	NA	NA	0.01	NA	0.0071	0.0231	56.4	32500	0.05	9.85	47	3000	742
9	1.59	1.11	0.69	0.63	328	334.25	6	113.0	NA	NA	NA	NA	0.0094	0.0265	46.5	26200	0.08	9.07	40	2500	418
10	2.12	1.37	0.64	0.64	320	327.85	8	91.4	NA	NA	-0.10	NA	0.0076	0.0234	62.0	35500	0.10	9.83	64	4100	503
11	1.30	0.45	0.35	0.38	321	329.29	8	99.8	100.2	99.7	-1.62	97	0.0080	0.0240	38.0	21700	0.10	9.70	72	4600	537

Table 2: Experimentally measured data and some key calculated variables for steady states achieved for category I (specified exit condition) partial condensation flows.

Run No.	\dot{M}_{in} (g/s)	\dot{M}_v (g/s)	Z_{e-exp}	T_w (K)	T_{sat} (K)	ΔT (K)	P_{in} (kPa)	P_{x6} (kPa)	P_{T^*} (kPa)	Δp (kPa)	P_{D2} (kPa)	ρ_2/ρ_1	μ_2/μ_1	G (kg/m ² s)	Re	Ja	Pr ₁	\dot{Q}_{out} (J/s)	q'' (W/m ²)	h (W/m ² K)
	±0.05	±0.04	±0.04	±1	±0.15	±1	±0.6	±0.6	±0.7	±0.05	±2	±0.0001	±0.0001	±1.5	±900	±0.02	±0.02	±5	±800	±80
1	1.44	0.52	0.36	320	331.91	12	108.8	110.9	108.0	-1.82	106	0.0087	0.0244	42.1	23800	0.15	9.59	78	4900	416
2	1.31	0.50	0.38	320	329.16	9	99.4	100.3	99.5	-0.43	98	0.0080	0.0238	38.4	21900	0.11	9.72	69	4400	505
3	1.34	0.59	0.44	320	328.55	9	97.4	98.4	97.3	-0.32	96	0.0078	0.0236	39.1	22400	0.10	9.76	64	4100	491
4*	1.80	0.64	0.36	323	330.53	8	103.9	105.9	104.4	-0.59	103	0.0083	0.0246	52.6	29900	0.09	9.50	97	6200	851
5*	1.92	1.00	0.52	323	329.64	7	101.0	103.3	101.7	-0.40	100	0.0081	0.0244	56.1	32000	0.08	9.55	78	4900	771
6	1.20	0.00	0.00	320	332.23	12	110.5	113.2	110.5	-0.80	108	0.0088	0.0245	35.0	19800	0.16	9.57	101	6400	514
7	1.22	0.44	0.35	320	331.71	12	108.0	110.6	108.0	-0.62	106	0.0086	0.0243	36.6	20200	0.15	9.62	66	4200	351
8*	1.93	1.15	0.60	322	325.21	3	87.15	NA	NA	-1.30	NA	0.0071	0.0231	56.4	32600	0.04	9.87	67	4300	1174
9	1.61	1.14	0.70	322	332.57	11	111.4	104.6	107.0	-0.87	103	0.0089	0.0250	47.1	26630	0.13	9.46	35	2200	212
10	1.67	1.37	0.82	322	331.45	10	105.8	98.6	100.8	-0.74	97	0.0085	0.0245	49.0	27800	0.12	9.57	16	1000	108
11	1.81	1.02	0.56	317	331.48	14	106.8	102.1	NA	-0.58	99	0.0085	0.0237	52.9	30000	0.18	9.80	54	3400	236
12	1.66	0.60	0.36	318	333.15	15	113.5	108.6	NA	-1.46	106	0.0090	0.0243	48.5	27400	0.20	9.66	88	5600	363
13	1.71	0.49	0.28	316	331.14	15	108.0	107.9	108.1	-2.10	105	0.0085	0.0237	50.1	28400	0.19	9.81	103	6500	441
14	1.30	0.65	0.50	320	326.34	6	90.5	92.1	90.5	-1.15	88	0.0073	0.0230	38.0	21800	0.08	9.90	56	3500	545
15	1.29	0.55	0.43	321	331.63	11	107.7	113.2	110.1	-1.60	107	0.0086	0.0245	37.7	21400	0.14	9.57	62	3900	366
16	1.31	0.76	0.58	321	331.07	11	105.8	109.1	105.8	-0.95	104	0.0084	0.0243	38.3	21700	0.13	9.62	46	2900	279
17	1.14	0.88	0.77	319	326.73	8	91.6	92.8	91.9	-0.14	90.4	0.0074	0.0230	33.5	19300	0.09	9.92	22	1400	186
18	1.39	0.64	0.46	318	329.01	11	98.9	101.3	98.4	-0.65	97.1	0.0079	0.0234	40.6	23200	0.14	9.85	64	4100	377

The experimental runs reported in the next section were taken after ensuring that: (i) representative runs were repeatable, (ii) the mass flow rates for partial condensation cases added up to satisfy mass balance, (iii) overall energy balance for the test section was satisfied i.e. $\dot{M}_{in} \cdot h_{fg} \approx \dot{M}_w \cdot C_{pw} \cdot \Delta T_w$, where, ΔT_w is the rise in the water temperature in the annulus surrounding the test-section, and (iv) various data were reasonable (based on simulation estimates) and consistent with one another. The experimentally obtained partial condensation cases in category II (unspecified exit) are listed in Table 1 with all the essential details including exit vapor quality Z_e (fourth column) and its value obtained from simulations (fifth column). Note that the fourth and fifth columns are in good agreement with one another. The corresponding partial condensation flow cases under category I (*specified* exit condition cases) are listed in Table 2. The discussion for these partial condensation flow results for exit condition categories I and II are given next.

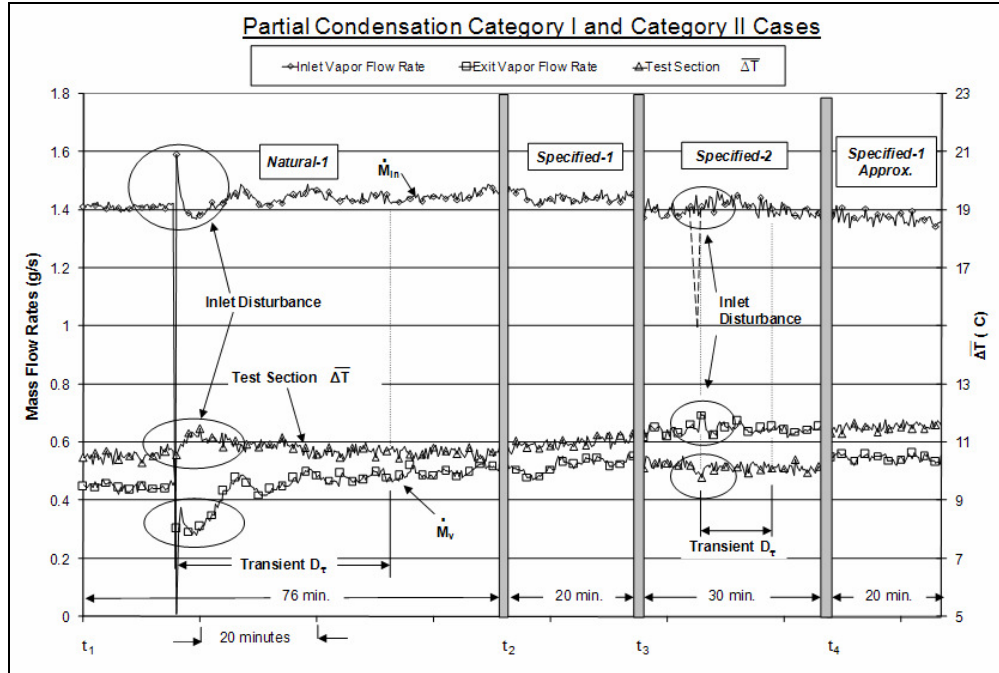


Fig. 9a: Time history depiction of \dot{M}_{in} , \dot{M}_v and ΔT values for multiple steady states of partial condensation cases viz. *Natural-1* (run 1 from Table 1), *Specified-1* (run 1 from Table 2), *Specified-2* (run 18 from Table 2), and *Specified-1 Approx.*

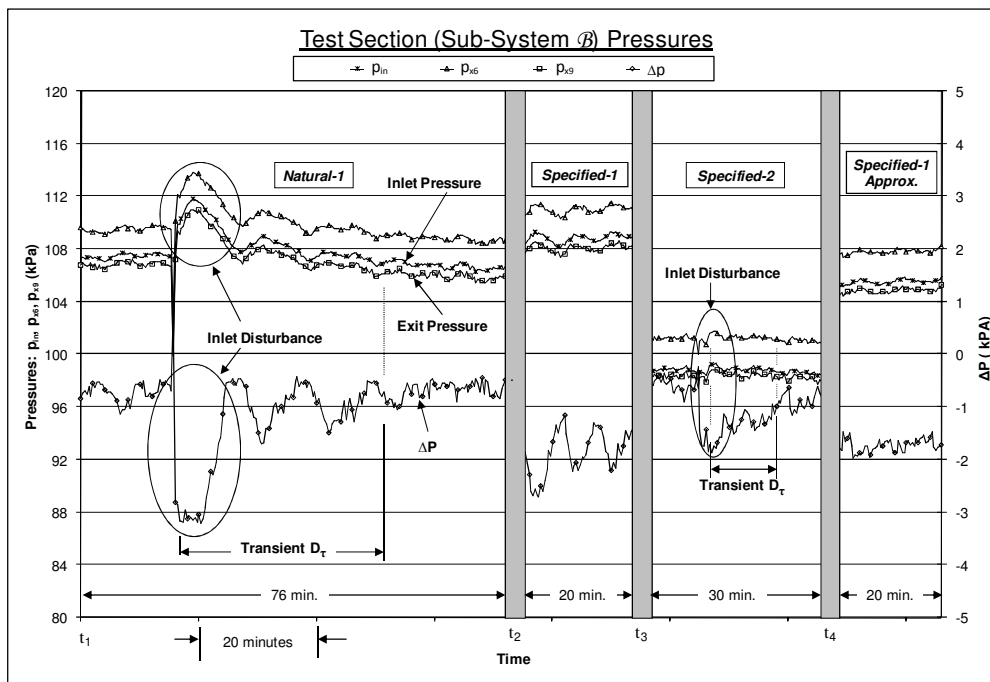


Fig. 9b: Time history of pressures (along the test section) and Δp values (across the test-section) for the cases shown in Fig. 9a.

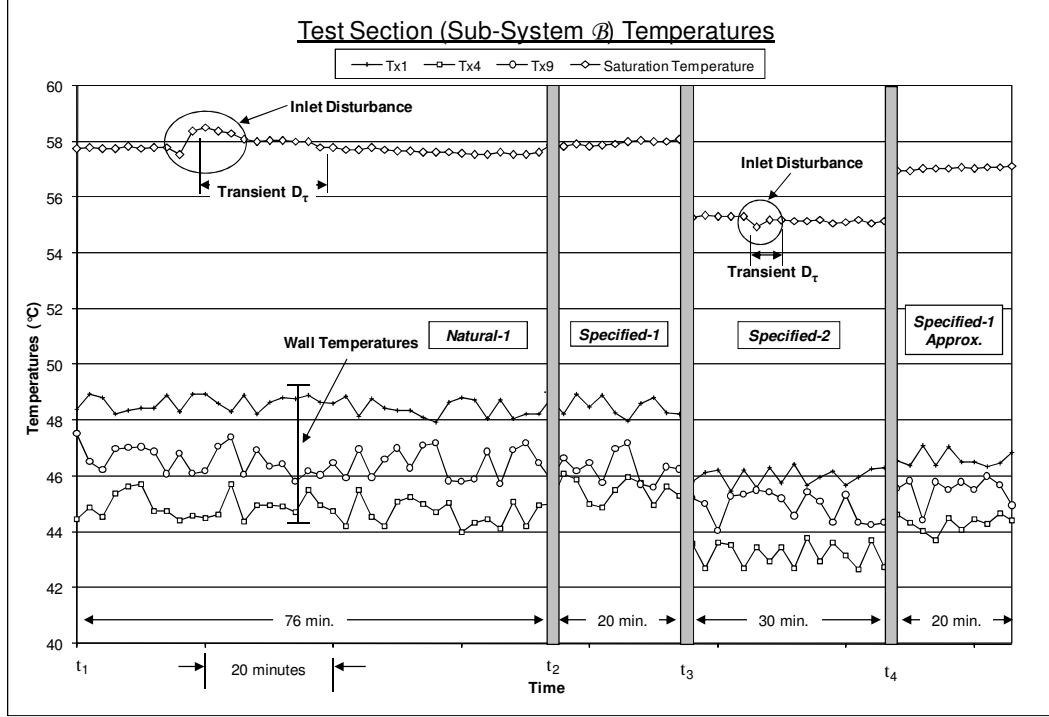


Fig. 9c: Time history of temperature values along the test section (sub-system B) and T_{sat} (p_{in}) for the cases shown in Fig. 9a.

Partial Condensation Flows

Specified Exit Condition (Category I) and Unspecified Exit Condition (Category II) Cases

The results over time interval $t_4 \leq t \text{ (min)} \leq t_4 + 20$, termed “Specified-1 Approx.” show the experiment’s ability to approximately repeat the data for a case that is approximately the same as the one for $t_2 \leq t \leq t_2 + 20$ termed *Specified-1*. Following the method described in section 3, Figs. 9a-9b also show, over the time interval $t_1 \leq t \text{ (min)} \leq t_1 + 76$, the attainment of a corresponding “natural” steady exit condition and associated steady flow variables for an unspecified exit condition (category II) case. This case corresponds to run 1 in Table 1. The *Natural-1*, *Specified-1* and *Specified-2* steady states (in Fig 9a – 9c) have the same values of $\dot{M}_{\text{in}} \approx 1.44 \pm 0.05 \text{ g/s}$ and $\overline{\Delta T} \approx 11 \pm 1^\circ\text{C}$ but different values of \dot{M}_L and \dot{M}_V that satisfy $\dot{M}_L l_1 + \dot{M}_V l_1 = \dot{M}_L l_2 + \dot{M}_V l_2 = \dot{M}_{\text{in}}$. The differences between the *Specified-1* and *Specified-2* cases are: (i) they have different heat transfer rates (since, energy balance gives: $\dot{Q}_{\text{out}} \approx \dot{M}_L h_{\text{fg}}$), the two cases respectively have approximate heat transfer rates of $78 \pm 4 \text{ W}$ and $64 \pm 4 \text{ W}$ and average heat transfer coefficients of $416 \pm 40 \text{ W/m}^2\text{-K}$ and $377 \pm 40 \text{ W/m}^2\text{-K}$, and (ii) different hydrodynamics – the signature of which is clear through corresponding computational simulations and, also, through the difference between experimentally obtained mean values of Δp for the two cases (they are, in Table 2, respectively, -1.82 kPa and -0.65 kPa). Furthermore, specified (category I) and unspecified (category II) flows have different dynamic responses to a disturbance (in Figs. 9a-9c, a disturbance was induced by momentarily shutting or decreasing the opening in the valve V_1 shown in Figs. 6-7). The difference in dynamic response is seen by comparing *Specified-2* and *Natural-1* cases for transients’ decay time D_τ

associated with exit vapor flow rate \dot{M}_v in Fig. 9a or D_τ associated with Δp in Fig. 9b. In Fig. 9a, the rapid shutting or closing of valve V_1 caused the indicated responses in \dot{M}_{in} time history. For the *Natural-1* case, this response is as shown in Fig. 9a but a more rapid response for *Specified-2* case is not captured by the resolution of the figure and it is indicated by a dotted line. With regard to dynamic responses to a disturbance – it is clear that *Specified-2* case of Fig. 9a (though it is farther from a “natural” case) is more stable than the case for *Natural-1* because its transients decay time D_τ is much shorter. In other words, “natural” steady states for unspecified exit conditions (category II) are generally more noise-sensitive because the exit, in category II cases is not as isolated from flow variations further downstream of it as is the exit for specified exit condition cases (category I) - and this causes additional lingering impact of noise arising from the flow variables in the exit zone. Time histories of pressure and temperature values in sub-system \mathcal{A} , \mathcal{C} , and \mathcal{D} for the cases in Figs. 9a-9c are not shown here for brevity but are available in Figs. 7d-7e of Narain et al. [34].

The cases shown in Fig. 9a-9c are representative runs taken from a set of partial condensation runs for specified (category I) and unspecified (category II) exit condition cases in Tables 1-2. The data matrix associated with these partial condensation category I and category II cases is best represented by Fig. 10. The test matrix for all partial condensation (including both the categories I and II) cases is limited by the system limits and flow regime boundaries indicated on the plane marked by inlet mass flow rate \dot{M}_{in} and temperature difference $\overline{\Delta T}$ values. Figure 10 shows all the partial condensation cases plotted on the two dimensional plane formed by \dot{M}_{in} and $\overline{\Delta T}$. These parameters were found to be the key variables controlling the dynamics of the condensing flows in the test section.

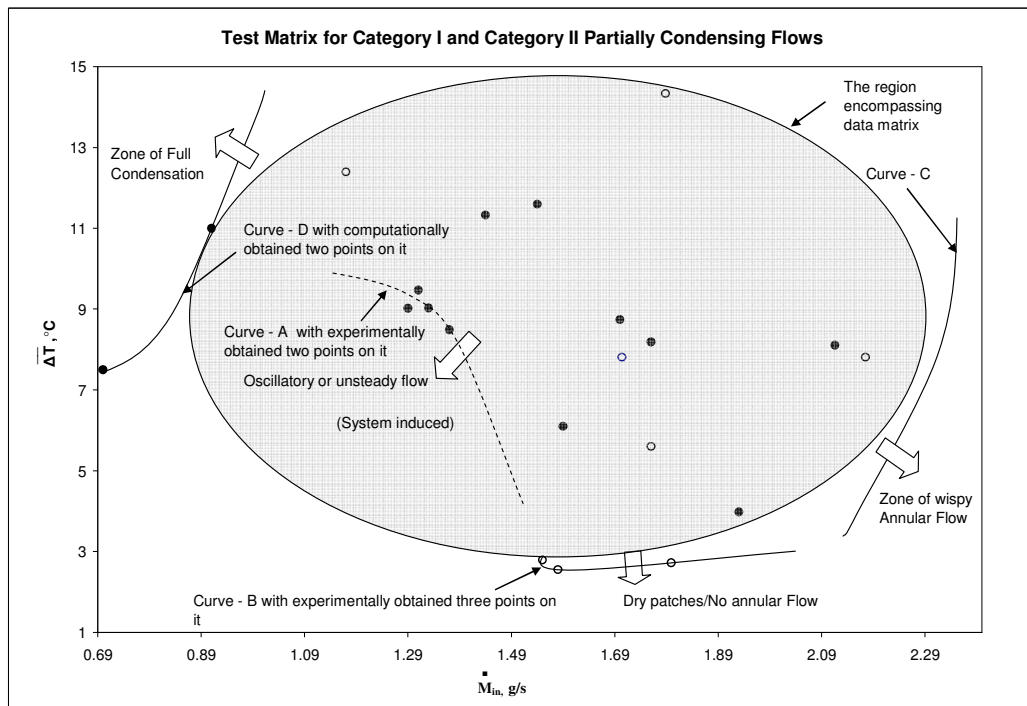


Fig. 10: Two-dimensional test data matrix for category II (unspecified exit condition) partial condensation cases' points and different bounding curves represented on \dot{M}_{in} - $\overline{\Delta T}$ plane.

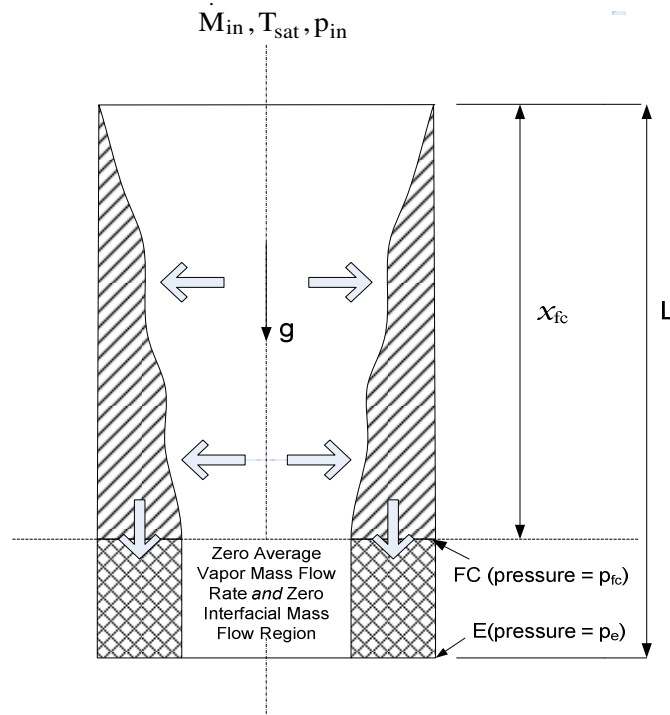


Fig. 11: The schematic of full condensation showing “point of full condensation” and its downstream region with zero interfacial mass and heat transfer.

The typical values for lower and upper limits for inlet mass flow rate were found to be 1 g/s and 2 g/s respectively and that for the $\overline{\Delta T}$ were recorded to be 2 °C and 12 °C respectively. The interior shaded zone in Fig. 10 represent \dot{M}_{in} and $\overline{\Delta T}$ values for which steady flows were attained for both specified (category -I) and unspecified (category II) exit condition cases. The bounding curve-B in Fig. 10 indicates lower threshold of $\overline{\Delta T}$ such that steady condensing flows attained below that curve (see points marked in Fig. 10) were drop wise patchy – i.e. not annular – on the condensing surface near the inlet. Below this curve, the condensation – as observed from the inlet boroscope – indicates that the flow is no more film annular near the point of onset of condensation as there are wet and dry patches associated with drop-wise condensation. This happens because $\overline{\Delta T}$ value is below a lower threshold. The bounding curve-B is partly experimental and curve-C on the right in Fig. 10 is, at present, entirely schematic (i.e. not fully explored by experiments). Curve-C represents expected transition to wispy-annular flows (see Fig. 10.3 in Carey [36]) at very high \dot{M}_{in} at any $\overline{\Delta T}$. The dotted curve-A on the left bottom has been experimentally noticed. This is a system-instability curve and does not represent a flow regime boundary for the test-section, as it is a result of the exit pressure oscillations or unsteadiness in test section imposed by oscillatory or other plug/slug instabilities occurring elsewhere in the system (in this case, in the auxiliary condenser downstream of the test section). An example of such an instability case is discussed in section 5. The bounding curve in the upper left corner of Fig. 10 is marked as curve-D. This curve represents transition from partial condensation to full condensation. If \dot{M}_{in} is reduced and $\overline{\Delta T}$ is increased further, computations show that the left side of curve-D represent the zone for which the entire vapor coming in condenses inside the test section (i.e., for category II flows, x_{fc} in the schematic

of Fig. 11 starts satisfying $x_{fc} \leq L$ on the left side of curve-D as opposed to $x_{fc} > L$ on the right side of curve-D). Note that Fig. 11 suggests, in accord with computations as well as remarks of Rabas and Arman [11], that this point of full condensation does not necessarily imply an all liquid phase for $x > x_{fc}$. It simply means that the zone $x > x_{fc}$ is such that average vapor mass flow rate \dot{M}_v is zero and so are the interfacial mass and heat transfer rates at these locations.

For a few data points in Fig. 10, the rotameter F_2 data was corrupted by the float's occasional stickiness to the rotameter walls. These cases are marked by unfilled circles in Fig. 10 and all the rest of the good cases (also based on comparisons with computational simulations) are marked by dark filled circles. These dark filled circles representing good partial condensation cases in Fig. 10 are actually the projections on the $\dot{M}_{in} - \overline{\Delta T}$ plane of the points reported in the three dimensional data matrix which has \dot{M}_{in} , $\overline{\Delta T}$ and $Z_e (\equiv \dot{M}_v / \dot{M}_{in})$ as three axes. This three-dimensional data matrix is not shown here for brevity but is shown in Fig. 8b of Narain et al. [34] where the figure is able to depict all the cases of category II (unspecified exit) as well as category I (specified exit) partial condensing flows. Each point in Fig. 10 represents, for given values of \dot{M}_{in} and $\overline{\Delta T}$, a set of data consisting both category I cases and its associated unique, "natural" category II case. There are, however, as seen in Fig. 8b of Narain et al. [34], some data sets representing only category I or category II cases. For each data set in Fig. 10 consisting of projections of category I and associated category II cases, category I flows were found to be more robust and stable as compared to their associated category II counterparts.

Comparisons with Relevant Computational Results (Partial Condensation)

Figure 12 shows the computationally obtained (employing the tools reported in [6]) details of local film thickness and heat flux variations for the specified and unspecified "natural" cases (under noise-free conditions) marked as *Specified-2* (run no. 18 in Table 2) and *Natural-1* (run no. 1 in Table 1) in Figs.

9a-9c. The variation of vapor quality $Z (\equiv \dot{M}_v / \dot{M}_{in}$ at any $x \equiv L_C \cdot x)$ along the test section can be easily

obtained from the graphical results in Fig. 12 from the relation $Z(x) \equiv 1 - \{(\pi \cdot D) / (\dot{M}_{in} \cdot h_{fg})\} \int_0^x q_w'' dx$.

The exit vapor quality for *Specified-2* case was greater than that of the associated *Natural-1* case. As a result, higher amount of vapor condenses for *Natural-1* case and this makes heat transfer rate \dot{Q}_{out} for *natural* case to be on the higher side (see Table 1 and 2 for details). For all other conditions remaining the same, as observed from the computational results in Fig. 12, this makes *Natural-1* case's liquid film thickness to be lower and wall heat flux to be higher than the values for *Specified-2* case.

Such details of representative local variations in film thickness and heat-flux are very important and should be more extensively synthesized with experimental results before heat-transfer correlations are developed for suitable categories and sub-categories of internal condensing flows. However, reliable experimental information on "local" spatial variations of these quantities is not expected until forthcoming incorporation of film thickness sensors and heat-flux sensors in these experiments. Observe that the computationally obtained prediction of "natural" exit vapor quality $Z_{e|Na\ Comp} (\approx 0.33)$ for category II flow in Fig. 9a-9c is in a very good agreement with the experimentally obtained $Z_{e|Na\ Expt} (\approx 0.33)$ value (see Table 1). In fact, a very good agreement between $Z_{e|Na\ Comp}$ and $Z_{e|Na\ Expt}$ values was found for all category II cases in Fig. 10 and this is clear from their numerical values in Table-1. Note that good agreement between experimental and theoretical Z_e values have also been obtained and

reported (see [5]) for shear driven condensing flow in a channel (category II experiments of Lu and Suryanarayana [37]) of gap height h and length L are such that $L/h \equiv x_e < x^*$, where x^* has the same meaning as in Fig. 3.

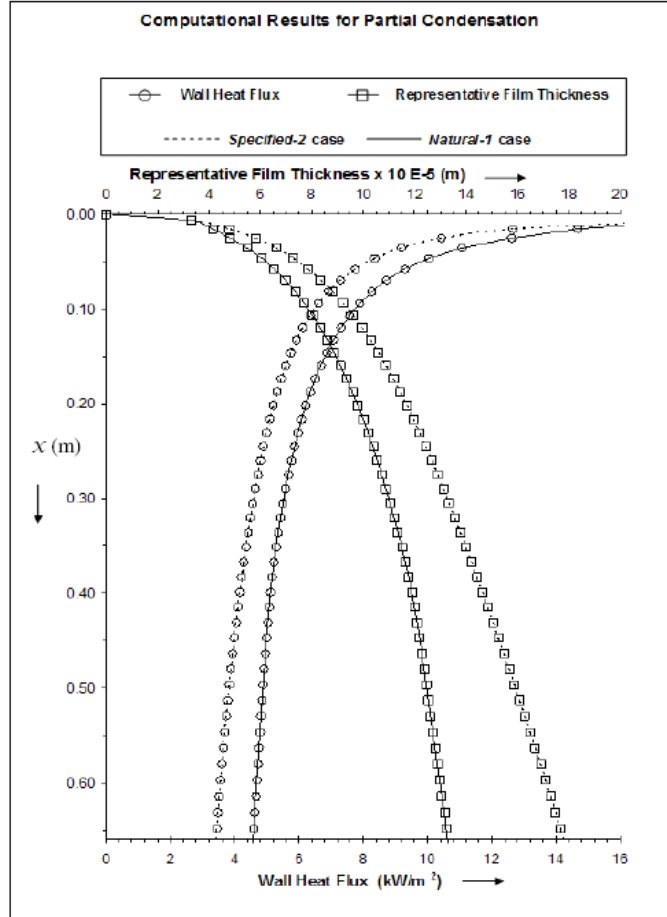


Fig. 12: For the “*Natural-1*” and “*Specified-2*” flow cases in Figs 9a-9c, this figure shows the computationally obtained representative film thickness and wall heat-flux variations along the test section. The film thickness and heat flux values shown have been obtained for smooth interface conditions. In reality, they are modulated by waves in presence of noise (see [6]).

The values of pressure drop Δp (given by $p_{in} - p_{exit}$) obtained from simulations for all the category II partial condensation cases were negative and below 50 Pa, indicating p_{exit} was greater than p_{in} for all the condensation cases in given \dot{M}_m range. Thus the pressure rises across the test-section. The pressure rise is needed to decelerate the vapor, feeding the gravitationally accelerated condensate at the rate needed for condensate motion under unspecified exit pressure condition. This is confirmed by the experimental values of Δp (see Tables 1 and 2) which are also all negative (except a very few cases). However, as expected, the magnitudes for experimental values of Δp were found to be greater than those from simulations. The reason behind this is that the simulations assume laminar vapor/laminar liquid flows while, in reality, the vapor Reynolds number are in the higher range (20000-30000); and this makes

vapor flows significantly turbulent in the core (see Tables 1-2), but still laminar near the interface. The turbulence in the vapor core does not affect the mass transfer across the interface by much because condensate motion is gravity driven and the flow of the condensate and near interface vapor is laminar in nature. However, turbulent vapor core significantly increases needed Δp values for the vapor domain while still keeping its impact on the gravity driven condensate motion negligible. Because of this, the values of vapor quality obtained from the simulation are in good agreement with the experiments but the values of pressure drop Δp obtained from experiments are higher in magnitudes than those predicted by the assumption of fully laminar vapor flows. However, predicted pressure drop Δp values do become comparable to experimental values if the predicted interface location is retained and k- ϵ model (see Narain et al. [34]) is used for the turbulent interior of the vapor while retaining the laminar shear stress estimates at the interface. The modifications in computational procedure needed to account for vapor turbulence are briefly discussed in Narain et al. [34].

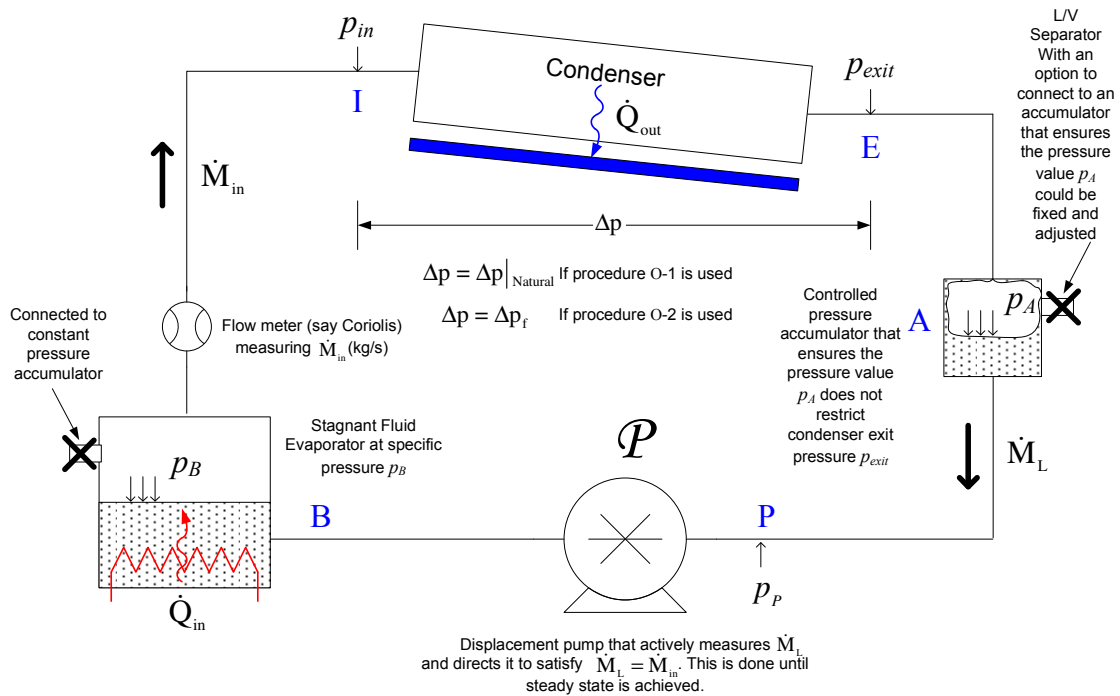


Fig. 13a: Specially designed ideal experimental arrangement. This is a specialized arrangement for a condenser (experiencing complete condensation) in a “thermal system” that transfers heat from a high temperature location to a low temperature location. The specialty of this arrangement is that it can be used to keep exit pressure of the condenser unspecified (by not using the accumulator option for A) or to specify it with precise control (by using the accumulator option for A). It should be noted that the pressure controlling accumulators, whether they are used for the evaporator B or the L/V separator A, accomplish their task by adjusting the amounts of vapor that is exchanged (come in and go out) between the accumulator and the liquid reservoir of interest (A or B).

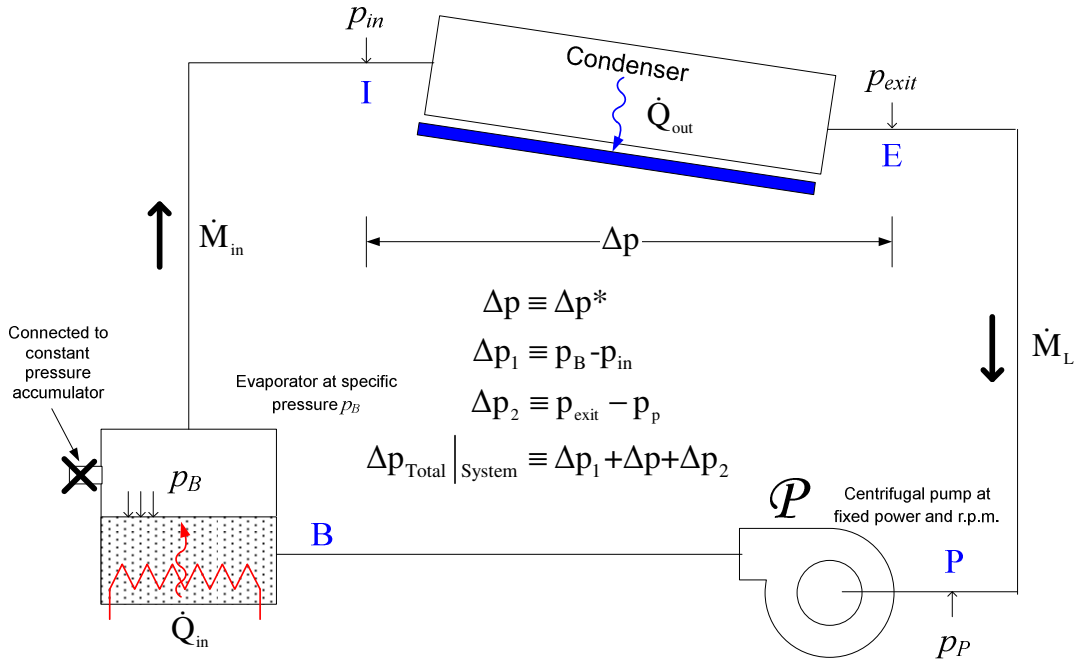


Fig. 13b: Example of an experimental arrangement for which condenser exit conditions are not directly controlled. This system, a variation of the system in Fig.13a, is again for a condenser (experiencing complete condensation) in a “thermal system” that transfers heat from a high temperature location to a low temperature location. This arrangement does not allow for the condensing flow to seek a natural pressure drop as the system decides this pressure drop. This is essentially a specified exit condition flow with the specification being decided by the system (see section 6).

Fully Condensing Flows

The experimental data and discussions for category II fully condensing flows are not reported here for brevity but can be found in Narain et al. [1]. The experimental investigations of fully condensing category I flows are currently in progress. However the essential ideas for these experiments are discussed here. For fully condensing flow cases the temperature difference $\overline{\Delta T}$ for a given inlet mass flow rate \dot{M}_m in the experimental set up of Fig. 7 is such that that there is zero mass flow through the depicted auxiliary condenser and, therefore, valve V_3 can be considered closed. For the case of unspecified exit pressures (category II flows), the flow loop in Fig. 7 makes available a range of exit pressures for the flow in the test-section by allowing a range of values for temperature T_{D1} in the L/V separator at point D_1 in the flow loop of Fig. 7. As a result, the pressure $p = p_{sat}(T_{D1})$ in the L/V separator can vary over a range because temperature T_{D1} can take any value between the ambient temperature and the temperature at the exit of the test-section. This special arrangement for fully condensing flows under unspecified exit pressure conditions at fixed boiler pressure p_B is best indicated by the simplified flow-loop in Fig. 13a where the L/V separator location is now marked by point A (instead of the marker D_1 used in Fig. 7). For the case discussed above, the L/V separator at point A in Fig. 13a is not connected to an active pressure controlling accumulator. In practice, many condensers employ this L/V separator by making it an integral part of the bottom portion (which is not cooled) of

the test-section condenser – this is effectively and practically achieved by using an orifice-plate (i.e. a significantly smaller diameter tube than the test-section) at the exit of the test-section. For specified exit pressure fully condensing flow cases (category I), besides the boiler in Fig. 13a, the L/V separator at point A is also connected to an “active” pressure controlling accumulator which holds the pressure fixed at a specified value.

For the complete condensation condenser in the system of Fig. 13a, an inadvertent design – which does not consciously keep the exit pressure specified or unspecified – is indicated in Fig. 13b.

5. RESULTS/COMMENTS ON SYSTEM INSTABILITIES AND OSCILLATORY FLOWS

While seeking the “natural” exit condition for some unspecified exit condition (category II) partial condensation flows, system instabilities – involving oscillatory flows – of the type shown in Figs. 14a - 14b are observed. The origin of these oscillatory flows appears to be the auxiliary condenser, which sees an approximate category III flow for which, in Fig. 6, the L/V separator at point D₁ is at approximately fixed stagnation pressure and the L/V separator downstream of the auxiliary condenser at point D₃ is at another approximately fixed stagnation pressure. These pressures respectively correspond to pressures $p_{\text{Tank-in}}$ and $p_{\text{Tank-out}}$ that appear in the definition given in section-1 for category III flows. Recall that these fully condensing flows in the auxiliary condenser, unlike the ones studied for the test section, are known (as in [14]) to become oscillatory under certain choices of pressures $p_{\text{Tank-in}}$ and $p_{\text{Tank-out}}$. Since complete auxiliary condenser flow data were not obtained (because this component was not the focus of the reported investigations), relating this auxiliary condenser instability to the type of stability boundaries discussed in [14] and [16] is outside the scope of this study.

It is clear from Figs. 14a-14b that oscillations in vapor mass flow rate at the exit of the test section impose oscillations on the exit pressure and on the pressure drop Δp across the test section while the inlet vapor mass flow rates remain relatively unaffected. Figure 14b shows the oscillations in other pressure values and the temperature at the rotameter F₂ (which is nearer to the auxiliary condenser). This, along with the known fact (see Fig. 9 in [4]) that there is one to one relation between exit vapor quality and exit pressure, indicate imposition of oscillatory pressures at the exit of the test-section.

It suffices here to note that the flow oscillations in the auxiliary condenser can induce an oscillatory exit pressure at the exit of the test-section condenser and this is the cause, in Figs. 14a-14b, of somewhat reduced level of oscillatory behavior of other test-section flow variables. As a result of the instability in the auxiliary condenser, the dotted curve-A in Fig. 10 is merely suggestive of the possible presence of system instabilities. This is because the actual onset of oscillatory conditions has only a very indirect and incomplete relation to test-section \dot{M}_{in} and $\overline{\Delta T}$ values used in Fig. 10.

The issues regarding start-up time for the flow loop are discussed in Narain et al. [34] and Kurita [33].

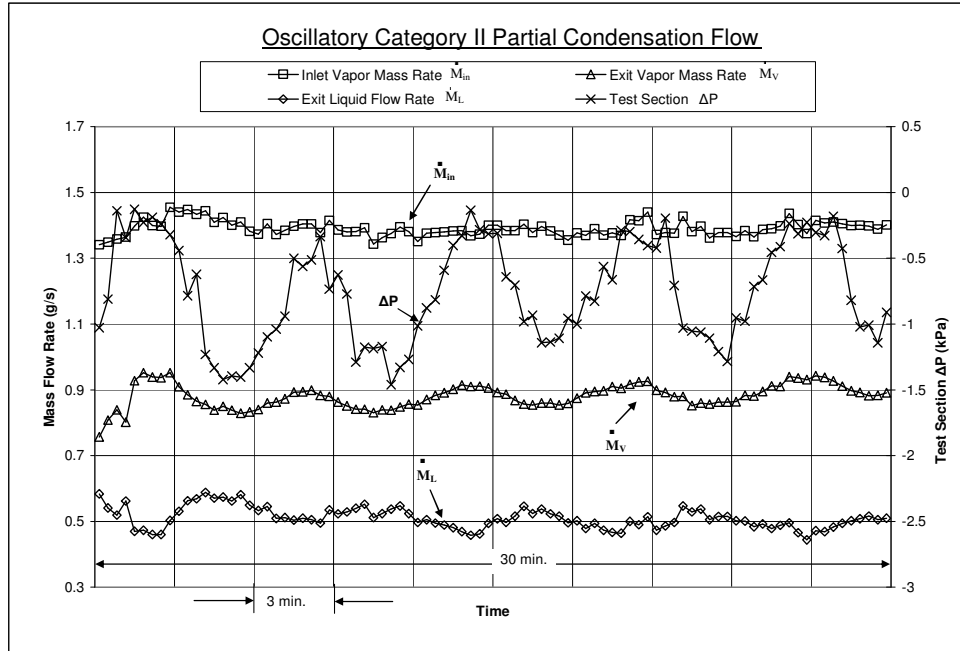


Fig. 14a: Time history depiction of \dot{M}_in , \dot{M}_v , \dot{M}_L and Δp values for an oscillatory partial unspecified exit condition case (category II). In Fig. 10, this flows' appearance is indicated by crossing of the dotted curve-A.

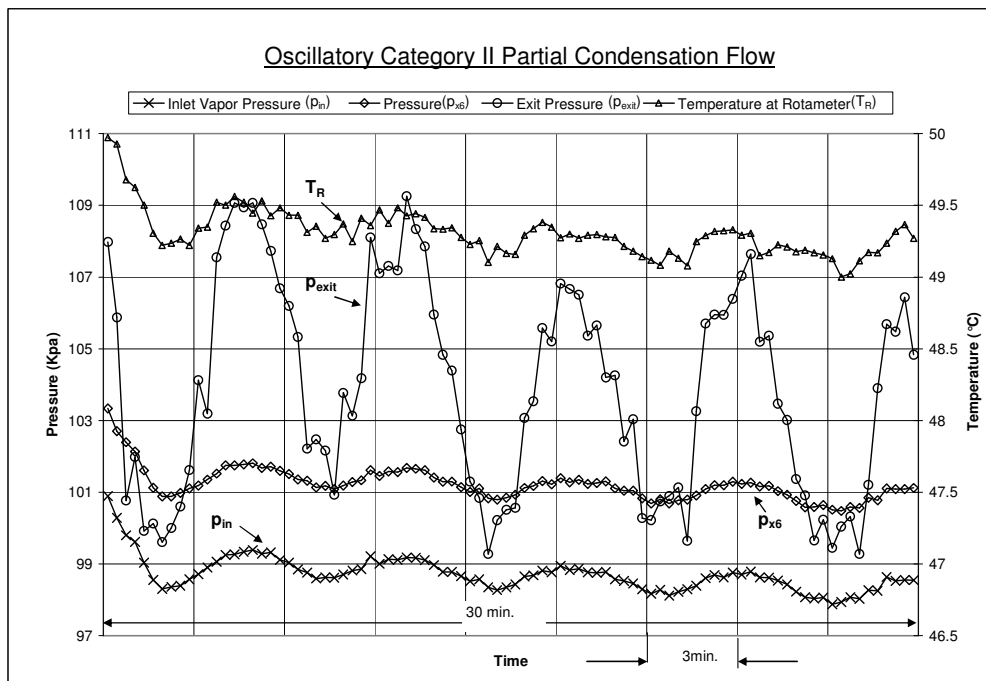


Fig. 14b: For the case in Fig. 14a, this figure shows the time history depiction of rotameter temperature T_R and the following pressures: inlet pressure p_{in} , pressure (p_{x6}) at location 6 in Fig. 7, and exit pressure p_{exit} .

6. EXIT CONDITION PARAMETER ϕ AND SUMMARIZED GENERALIZATIONS OF RESULTS FOR THIS AND OTHER INTERNAL TWO-PHASE FLOWS

As discussed above, pressure difference $\Delta p = p_{in} - p_{exit}$ in Fig. 13a, is typically not well defined for condensing duct flows just by the virtue of specified inlet and wall conditions alone - though it is well defined for single phase fluid flows. This is because outlet pressure often needs to be prescribed as a boundary condition to determine the flow field in the interior and the associated pattern of gas-liquid interfacial configurations in phase-change flows. The above stated conclusion for condensing flows, is also true, for many boiling flows - particularly if changes in interface location near the heat transfer surfaces (at specified wall temperatures) can be easily accommodated by significantly changing the interfacial mass-flux (and heat-flux) conditions. The reason behind the significance of exit pressure for these flows is that changes in exit pressure p_{exit} tries to change the gas-phase squeezing pressure levels $(p_{in} + p_{exit})/2$ and, concurrently, vapor motion due to different $\Delta p = p_{in} - p_{exit}$ values that are being imposed. Even small changes in these two factors (i.e. mean pressure level and pressure difference from inlet to exit of two-phase component) can be accommodated by phase-change flows because of the extra degree of freedom associated with various liquid-vapor interface configurations (flow morphologies) that are easily altered by changing the interfacial mass-flux (and associated wall heat-flux) assuming cooling/heating is done at fixed wall temperatures (not fixed heat-fluxes).

However, historically, exit pressure specification has not been considered because of an incorrect and untested assumption that *all* two phase flow components behave similar to single phase flow components with regard to pressure drop across the component. As a result of this misunderstanding, for many “systems” in application, the pressure difference Δp across a two-phase component gets inadvertently specified or is subjected to large system imposed variations in Δp . This leads to difficulties in experimentally characterizing two-phase flow behavior. Because of this, characterization of two-phase flow behavior of a condensing or flow boiling component in a system cannot easily be decoupled from the system and, therefore, due consideration should be given to the manner in which the component is integrated in the system hardware. All this requires a paradigm change from seeking a correlation for pressure difference Δp to first assessing the value or range of externally imposed Δp values. Only after this assessment, one can meaningfully develop and use suitable heat-transfer correlations.

In the context of the results reported in section-1, when exit pressure is left unspecified (category II flow) through specially designed experimental arrangements, the flows further fall in the following two sub-categories, namely: (A) the ones for which a well defined steady “natural” pressure-difference “ $\Delta p|_{Natural}$ ” and associated “natural” interfacial configuration exist, and (B) the flows for which well defined steady “natural” pressure-difference “ $\Delta p|_{Natural}$ ” and associated “natural” interfacial configuration do not exist. An example of “natural” flow of type (A) is gravity dominated condensing flows or some upstream portions ($x < x^*$) of shear driven flows. However, in practice, type (A) flows are seldom realized in gas-liquid flow components/test-sections unless the system is especially designed to offer freedom to choose exit pressures. This is because, if the condenser is not integrated in a specially designed system, an example of which is the system shown in Fig. 13b, then the flow is either unable to seek “ $\Delta p = \Delta p|_{Natural}$ ” value due to exit pressure constraints or it gets inadvertently specified. Examples

The mass flow rate $\dot{M}_{in} = \dot{Q}/h_{fg}(p_B)$ (where h_{fg} is the *heat of vaporization* of the pure fluid employed in the system) is held fixed along line AB of Fig. 15a by the fixed heat load \dot{Q} and a fixed pressure p_B for the evaporator/boiler. In many practical applications, however, the line AB is a band which accounts for changing heat loads \dot{Q} as well as changes in steady boiler pressure p_B (which is often not held fixed by an accumulator).

The unspecified pressure p_{exit} case – procedure O-1

As stated earlier, pressure $p_A \approx p_{sat}(T_A)$ for nearly stagnant liquid in the accumulator A (in Fig. 13a) is allowed to vary in a range determined by the range of allowed temperatures T_A . This degree of freedom for pressure p_A is typically sufficient –except for some cases (see an example in [1]) - for the two-phase condensing flow to be able to vary its exit pressure “ p_{exit} ” and seek its “natural” value “ $p_{exit|Natural}$.” As shown in Fig. 15a, this attainment of $\Delta p|_{Natural}$ is achieved at the intersection of the line AB and the well defined curve C that exists for type (A) flows in this category. The curve C represents a function $\Delta p|_{Natural} = f(\dot{M}_{in})$ for a given inlet pressure p_{in} and vapor to condensing-surface temperature difference $\Delta T(x)$. For each \dot{M}_{in} , the system design allows the flow in test section to have sufficient freedom in selection of Δp values and this is indicated by converging arrows at the intersection point D in Fig. 15a. Note that these curve C flows do not exist for many type (B) flows common to fully condensing microgravity situations (with $x_e > x^{**}$ in Fig. 3) as no steady flow can be realized.

The specified exit pressure p_{exit} case – procedure O-2

Different pressure levels p_A in the L-V separator of Fig. 13a are fixed by connecting it to the accumulator which employs active heating/cooling. This active heating/cooling of the accumulator is accomplished by a feedback control process using thermo-electric coolers and electric heaters controlled by suitable electronics, software, and a computer. These different fixed values of p_A correspond to different fixed values of p_{exit} and $\Delta p \neq \Delta p|_{Natural}$ – and this is indicated by Δp_f in Fig. 15a. Therefore resulting flows are in the specified exit pressure category (category I). This operational procedure allows us the choice to fix any value of Δp_f leading to essentially incompressible vapor flow (if Δp_f is fixed within the 1% compressibility band) or a flow with significant vapor compressibility (as shown in Fig. 15a). The compressible flows in this category require identification of another curve C_4 in Fig. 15a – because flows to the top and right of C_4 are likely to exhibit compressibility induced instabilities (such as oscillatory flows).

As indicated earlier, for a 0g or horizontal category II flow in a condenser of a given length L, there exists \dot{M}_{in-cr} and hence a curve C_3 in Fig. 15a needs to be demarcated. Only for flows to the top and right of this curve one has $\dot{M}_{in} > \dot{M}_{in-cr}$. Only under these conditions, one can ensure $x_e < x^*$ for category II flows or suitably specify Δp for category I flows.

Definition and Importance of Exit Pressure Parameter ϕ

It is clear from the above discussion that for unspecified exit condition cases, type (A) condensing flows can be realized with $\Delta p_{actual} = \Delta p|_{Natural}$ under a suitable experimental arrangement whereas type (B) flows will remain ill defined. On the other hand, for many condensing flows in the systems, Δp may be intentionally (as for Fig. 13a) or inadvertently (as for the system in Fig. 13b) specified. To

assess/predict condensing flows in this specified Δp category it is important to know the relation between Δp_{actual} and a certain reference pressure Δp_{Ref} . The relationship between Δp_{actual} and Δp_{Ref} is characterized by a non-dimensional exit pressure parameter:

$$\varphi \equiv \Delta p_{actual} / \Delta p_{Ref}. \quad (3)$$

If the corresponding flow under unspecified exit condition is type (A) – that is $\Delta p_{Natural}$ exists – we set $\Delta p_{Ref} = \Delta p_{Natural}$. If the corresponding flow under unspecified exit condition is type (B) – that is $\Delta p_{Natural}$ does not exist - we set $\Delta p_{Ref} = f_{known}(\dot{M}_{in})$ to be a fixed number (e.g. 1 kPa) through a pre-defined function f_{known} of \dot{M}_{in} . It is recommended that the definition of this function f_{known} be chosen such that the resulting curve also lies (as does curve C) within the feasible curves (between curves C3 and C4) and furthermore, nearly incompressible zone bounded by the curves C_1 and C_2 in Fig. 15a.

The above definition means that, for “natural” flows defined by type (A), the value of $\varphi = 1$. Also, with the above choice of Δp_{Ref} , $\varphi \approx 1$ signifies nearly incompressible flows for all specified exit pressure flow categories as well.

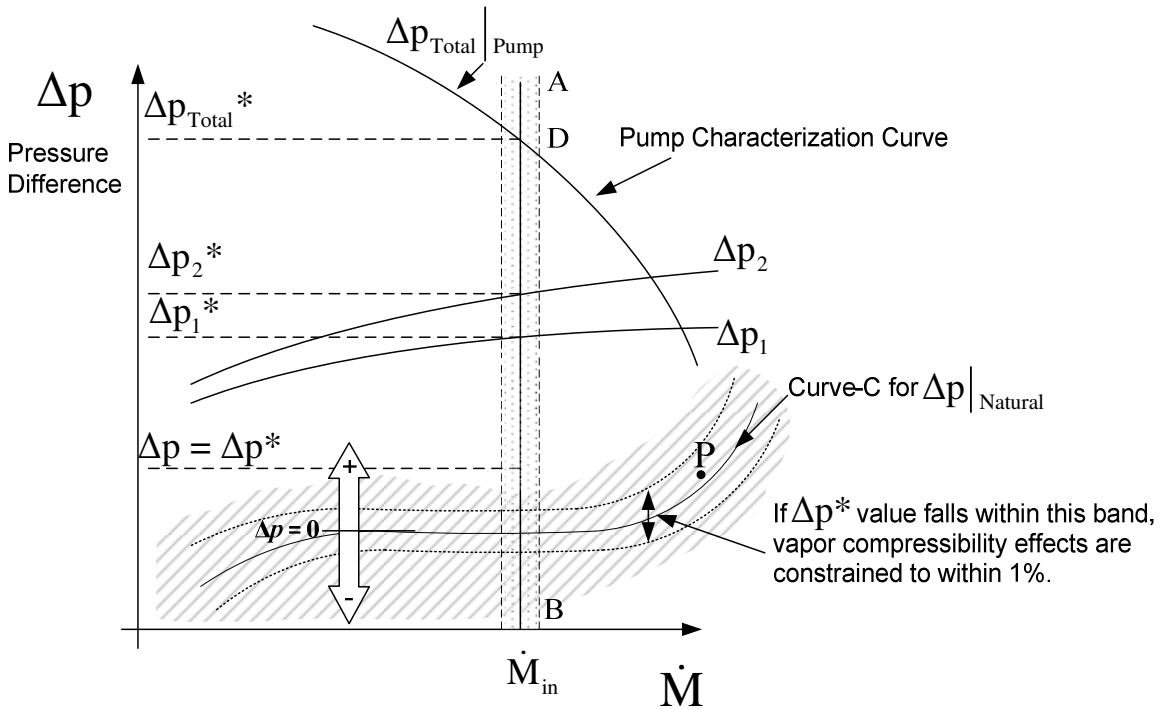


Fig. 15b: This figure shows the system and subsystem curves for condensing flow arrangement in Fig. 13b. The values Δp_{Total}^* , Δp_1^* , Δp_2^* are decided by intersection of the line AB and various curves. $\Delta p_{Natural}$ vs \dot{M} curve for the condenser is the same curve shown in Fig. 15a that would have been obtained if the flow was realized under arrangement shown in Fig. 13a. The pressure drop across the condenser Δp^* could be anywhere - its value being fixed by the system through the equation $\Delta p^* = \Delta p_{Total}^* - (\Delta p_1^* + \Delta p_2^*)$. The band around $\Delta p_{Natural}$ vs \dot{M} curve shows that if Δp^* falls within that band vapor compressibility effects will be small.

Determination of the Range of ϕ in Other Arrangements for Condensing Flows

Fig 13b shows a representative arrangement for condensers employed in different applications where the exit condition is unknown and inadvertently specified. Instead of a displacement pump, a centrifugal pump is used to pump liquid flow back to the evaporator. The main difference between arrangements in Figs. 13a and 13b is that, in Fig. 13b, the accumulator-cum-L/V separator is missing in the liquid line between the condenser exit and the pump. This means as opposed to the arrangement in Fig. 13a, the two-phase flow in the condenser is not decoupled from single phase heavier fluid flow. The system and sub-system curves for the arrangement in Fig. 13b are shown by the schematic in Fig. 15b. Similar to the arrangement in Fig. 13a, the mass flow rate \dot{M}_{in} in the system is assumed to be fixed along line AB shown in Fig. 15b (or in a narrow band around it) for fixed heat load \dot{Q} and a fixed pressure p_B for the boiler. As shown in Fig. 13b, the pressure difference between points B and P (as the flow goes through points I and E) is given by $\Delta p_{Total|_{System}}$. This can be split in to pressure drops across sub-systems identified in Fig. 13b as:

$$\Delta p_{Total|_{System}} = \Delta p_1 + \Delta p + \Delta p_2 \quad (4)$$

where, as shown in Fig. 13b, $\Delta p_1 = p_B - p_{in}$, $\Delta p = p_{in} - p_{exit}$, and $\Delta p_2 = p_{exit} - p_P$. Also, in Fig. 15b, for single phase fluid flows, Δp_1 and Δp_2 values are well defined functions of \dot{M} because they are pressure differences for single-phase flow regions. For the two-phase condenser, pressure difference Δp is not a well defined function of \dot{M} and this fact is being represented by a shaded zone in Fig. 15b. Furthermore, in Fig. 15b, $\Delta p_{Total|_{Pump}}$ is the value of the pressure difference “ $p_B - p_P$ ” as the flow goes across the pump. The $\Delta p_{Total|_{Pump}}$ curve in Fig. 15b is, however, obtained for the centrifugal pump by a separate characterization experiment in which the pressure difference “ $p_B - p_P$ ” is measured as the liquid flows through the pump at different mass flow rates \dot{M} . The steady mass flow rate $\dot{M} = \dot{M}_{in}$ achieved by this system is given by the intersection of line AB and the pump characterization curve $\Delta p_{Total|_{Pump}}$ in Fig. 15b.

At this intersection point in Fig. 15b, $\Delta p_{Total|_{Pump}} = \Delta p_{Total}^*$. Furthermore, the system requires that at this \dot{M}_{in} , the pressure difference between points P and B be the same whether it is obtained by the flow (along B, I, E, and P) through the system or through the pump from P to B (as given by the pump curve). This means $\Delta p = \Delta p^*$ value actually achieved must be such that it satisfies

$$\Delta p_{Total|_{Pump}} = \Delta p_{Total|_{System}} \quad (5)$$

leading to $\Delta p^* = \Delta p_{Total}^* - \Delta p_1^* - \Delta p_2^*$ where Δp_1^* and Δp_2^* are also as shown in Fig. 15b. This means for the arrangement shown in Fig. 13b, the condition at the exit of the condenser is essentially a specified exit pressure flow condition (category I). In these kinds of practical arrangements, the value of ϕ is at the mercy of the system and is generally not known unless the above type of analysis is done and $\phi \equiv \Delta p^* / \Delta p_{Ref}$ is computed.

If the condenser in Fig. 13b is properly sized to ensure that, over the range of ϕ values involved, the condenser actually achieves complete condensation then the remaining parts of the system in Fig. 13b can be made insensitive to the complexities of various flow regimes inside the condenser. For this special design, the curves representing Δp_1 , Δp_2 vs \dot{M} in Fig. 15b must have high slopes and satisfy: $|\Delta p_1| \sim |\Delta p_2| \gg |\Delta p|$. However, for proper designs of all such systems, one still needs to have good estimate of the range of ϕ values involved.

Addition of an L/V separator (without the accumulator shown in Fig. 13a) at the exit of the

condenser section of Fig. 13b has also been used by others (see [37]). While this may allow attainment of natural unspecified exit condition steady flows, the start-up time is significantly larger (about 12 hours in [37] as opposed to about 20 minutes in [1]) than those associated with the system in Fig. 13a that employs a displacement pump. This is because the centrifugal pump in Fig. 13b seeks the correct mass flow rate \dot{M}_{in} while strongly affecting the pressure in L/V separator (without the accumulator).

Impact of ϕ on Flow Regime Transition Boundaries for Condensing and Other Two-phase Flows

It should be noted that the results described above are mainly applicable to condensing flows as these new ideas were developed by our group after extensive experimental/computational research on condensing flows. Even then, relevant ideas may also be extended to other two phase flows namely, boiling, adiabatic gas-liquid flows, etc.

For a typical operating point P, in Fig. 15a and Fig. 15b, the entire condenser in the system is characterized by Δp , \dot{M} , $\Delta T(x)$ values. However, for flow within the condenser, for same set of these three parameters, there exist different flow regimes viz. annular, plug/slug, bubbly etc. Within the condenser, transition curves for these important flow regime boundaries (see [36]-[42]) – for given function $\Delta T(x)$ - are generally defined as curves in “ $\dot{M}_{in} - Z(x)$ ” space where vapor quality $Z(x)$ is defined as a ratio of cross sectional vapor mass flow rate of \dot{M}_v to \dot{M}_{in} and takes a value of one at the inlet and zero at the exit. In the light of the results presented above, these transition boundaries are significantly affected by the parameter ϕ and must be sought - for given function $\Delta T(x)$ – as surfaces in “ $\dot{M}_{in} - \phi - Z(x)$ ” space.

The above remarks about the impact of variable ϕ also clearly apply to flow boiling with sufficiently large exit vapor qualities.

For adiabatic two-phase flows, though $Z(x)$ is constant along x in a two-phase test section, the flow regime boundaries are expected to vary because ϕ is expected to vary (in a small neighborhood of $\phi = 1$) in “ $\dot{M}_{in} - \phi - Z(x)$ ” space. Though the variations in ϕ may be small from one experiment to another, the variations are expected to have a larger impact, particularly, on the location of the boundaries for the plug/slug and bubbly regimes. This may explain why ([42]) the available empirical correlations for Δp as a function of \dot{M}_{in} and $Z(x)$ are good in the interior of flow regime boundaries but not so good on the more poorly defined flow regime boundaries.

7. CONCLUSIONS

- This paper experimentally confirms the significance of exit conditions on the nature of quasi-steady internal condensing flows and proposes a novel and necessary exit-condition based categorization of these flows.
- In particular, for gravity driven condensate flows, experimental procedures and results for achieving steady and stable partial condensing flows under specified and unspecified exit conditions is presented here. In section 6, corresponding procedures for fully condensing flows are described.
- The experiments reinforce simulation results that, for partial condensation, multiple steady states, with quite different local and average heat transfer rates, are often achieved under different exit condition specifications (category I flows). Therefore, correlations for heat transfer coefficient (though not developed here) are only meaningful if flow regimes are clearly defined and developed in the framework of proposed exit-condition based categories.

- The existing simulation tool’s ability to be quantitatively correct in identifying “natural” exit conditions for gravity driven partial condensation cases under unspecified exit conditions (category II) is very good as this is supported by the reported experiments. This agreement adds credibility to the experimental results, simulation tool, and the proposed exit condition based categorizations.
- The transients in partial condensation experiments establish that the steady flows are definitely more robust under specified exit condition (category I) operation of condensers. This lends credibility to the simulation result that steady operation of shear driven condensers (in zero gravity and horizontal configurations) are much more difficult to achieve under unspecified exit conditions (category II). In general, these results suggest that specified exit-condition flows (category I flows) – for both partial and complete condensation cases - with properly selected exit pressure values are likely to be more robust and more readily realized than flows under other arrangements (category II or category III under arbitrarily fixed pressures and valve settings).
- Some flow regime and system boundaries for annular category I and category II flows are observed and reported here. Though these reported preliminary identifications of flow regime boundaries need to be made more definitive, their identifications are clearly important for attaining or ascertaining steady performances of condensers.
- This paper generalizes the above results and identifies a parameter ϕ , whose proper accounting is important for characterizing most forced internal duct phase-change flows.
- The experiments clearly demonstrate the difference between flow regime boundaries and system-instability boundaries and the importance of identifying system-instability boundaries that are specific to individual systems. For example, curve A in Fig. 10 represents, system instability boundaries that arise from restrictions imposed on the exit pressure by phenomenon occurring in components downstream of the test section.

8. APPENDIX

Channel Flow Governing Equations

The liquid and vapor phases in the flow (e.g. see Fig. 1) are denoted by a subscript I: I = 1 for liquid and I = 2 for vapor. The fluid properties (density ρ , viscosity μ , specific heat C_p , and thermal conductivity k) with subscript I are assumed to take their representative constant values for each phase (I = 1 or 2). Let T_I be the temperature fields, p_I be the pressure fields, $T_s(p)$ be the saturation temperature of the vapor as a function of local pressure p , Δ be the film thickness, \dot{m} be the local interfacial mass flux, $T_w(\mathbf{x}) (< T_s(p))$ be a *known* temperature variation of the cooled bottom plate, and $\mathbf{v}_I = u_I \hat{\mathbf{i}} + v_I \hat{\mathbf{j}}$ be the velocity fields. The flow fields are defined at every point \mathbf{x} (a 3-D Euclidean position vector) and time t . Furthermore, let h be the channel height, g_x and g_y be the components of gravity along x and y axes, p_0 be the inlet pressure, $\Delta T \equiv T_s(p_0) - T_w(0)$ be a representative controlling temperature difference between the vapor and the bottom plate, h_{fg} be the heat of vaporization at temperature $T_s(p)$, and U be the *average* inlet vapor speed determined by the inlet mass flux. With t representing the actual time and (\mathbf{x}, \mathbf{y}) representing physical distances of a point with respect to the axes for the channel flow ($\mathbf{x} = 0$ is at the inlet, $\mathbf{y} = 0$ is at the condensing surface, and $\mathbf{y} = h$ is an isothermal slightly superheated non-condensing surface), we introduce a new list of fundamental non-dimensional variables – viz. $(x, y, \tau, \delta, u_1, v_1, \pi_1, \theta_1, \dot{m})$ - through the following definitions:

$$\begin{aligned} \{\mathcal{X}, \mathcal{Y}, \Delta, u_i, \dot{m}\} &\equiv \{h \cdot x, h \cdot y, h \cdot \delta, U \cdot u_i, \rho_i \cdot U \cdot \dot{m}\} \\ \{v_i, T_i, p_i, t\} &\equiv \{U \cdot v_i, (\Delta T) \cdot \theta_i, p_0 + \rho_i U^2 \cdot \pi_i, (h/U) \cdot \tau\}. \end{aligned} \quad (\text{A.1})$$

Interior Equations

The non-dimensional differential forms of mass, momentum (x and y components), and energy equations for incompressible flow in the interior of either of the phases are the well-known equations:

$$\begin{aligned} \frac{\partial u_i}{\partial x} + \frac{\partial v_i}{\partial y} &= 0 \\ \frac{\partial u_i}{\partial \tau} + u_i \frac{\partial u_i}{\partial x} + v_i \frac{\partial u_i}{\partial y} &= - \left(\frac{\partial \pi_i}{\partial x} \right) + Fr_x^{-1} + \frac{1}{Re_i} \left(\frac{\partial^2 u_i}{\partial x^2} + \frac{\partial^2 u_i}{\partial y^2} \right) \\ \frac{\partial v_i}{\partial \tau} + u_i \frac{\partial v_i}{\partial x} + v_i \frac{\partial v_i}{\partial y} &= - \left(\frac{\partial \pi_i}{\partial y} \right) + Fr_y^{-1} + \frac{1}{Re_i} \left(\frac{\partial^2 v_i}{\partial x^2} + \frac{\partial^2 v_i}{\partial y^2} \right) \\ \frac{\partial \theta_i}{\partial \tau} + u_i \frac{\partial \theta_i}{\partial x} + v_i \frac{\partial \theta_i}{\partial y} &\approx \frac{1}{Re_i Pr_i} \left(\frac{\partial^2 \theta_i}{\partial x^2} + \frac{\partial^2 \theta_i}{\partial y^2} \right), \end{aligned} \quad (\text{A.2})$$

where $Re_i \equiv \rho_i U h / \mu_i$, $Pr_i \equiv \mu_i C_{p_i} / k_i$, $Fr_x^{-1} \equiv g_x h / U^2$ and $Fr_y^{-1} \equiv g_y h / U^2$.

Interface Conditions

The nearly exact interface conditions (see Delhaye [43]) for condensing flows are used. Utilizing a superscript “i” for values of flow variables at the interface $\mathcal{H}(\mathbf{x}, t) = \mathcal{Y} - \Delta(\mathcal{X}, t) = 0$, the unit normal at any point on the interface, directed from the liquid towards the vapor, is denoted by $\hat{\mathbf{n}}$ and is equal to $\nabla \mathcal{H} / |\nabla \mathcal{H}|$. Here, “ ∇ ” and “ ∇_s ” respectively denote 3-D (in Euclidean space) and surface 2-D (on curved surface of the interface) gradient/divergence operators depending on whether they are acting on scalar/vector fields. The unit tangent at any point on the interface, directed towards increasing \mathcal{X} , is denoted by $\hat{\mathbf{t}}$. The velocity \mathbf{v}_s of a point on the dynamic interface is such that it satisfies the well known kinematic restriction: $\mathbf{v}_s \cdot \hat{\mathbf{n}} = (-\partial \mathcal{H} / \partial t) / |\nabla \mathcal{H}|$. Each phase is modeled as a viscous and incompressible Newtonian fluid with stress tensor $\mathbf{T} = -p_i \mathbf{1} + \mathbf{S}_i$ where viscous stress tensor $\mathbf{S}_i = \mu_i \{(\text{grad} \cdot \mathbf{v}_i) + (\text{grad} \cdot \mathbf{v}_i)^T\} / 2$ and $\mathbf{1}$ is the identity tensor. The interface conditions and their non-dimensional forms are given below.

- The tangential component of the vapor and liquid velocities at the interface must be continuous, i.e.
$$\mathbf{v}_1^i \cdot \hat{\mathbf{t}} = \mathbf{v}_2^i \cdot \hat{\mathbf{t}}. \quad (\text{A.3})$$

The non-dimensional Cartesian form of the above requirement for the channel flow of interest becomes:

$$\mathbf{u}_2^i = \mathbf{u}_1^i - \delta_x (v_2^i - v_1^i), \quad (\text{A.4})$$

where $\delta_x \equiv \partial\delta/\partial x$.

- Ignoring normal component of $\nabla_s \sigma$ and viscous stresses in the first equality, the second equality given below models the normal component of momentum balance at a point on the interface. That is:

$$\begin{aligned} p_1^i &= p_2^i + \dot{m}^2(1/\rho_2 - 1/\rho_1) + \sigma \nabla_s \cdot \hat{\mathbf{n}} - \nabla_s \sigma \cdot \hat{\mathbf{n}} + (\mathbf{S}_1^i - \mathbf{S}_2^i) \hat{\mathbf{n}} \cdot \hat{\mathbf{n}} \\ &\cong p_2^i + \dot{m}^2(1/\rho_2 - 1/\rho_1) - (\sigma \Delta_{xx}) / [1 + \Delta_x^2]^{2/3}. \end{aligned} \quad (\text{A.5})$$

The non-dimensional Cartesian form of the above requirement for the channel flow of interest becomes:

$$\pi_1^i = \frac{\rho_2}{\rho_1} \pi_2^i - \frac{1}{\text{We}} \left(\frac{\delta_{xx}}{[1 + \delta_x^2]^{3/2}} \right) + \dot{m}^2 \left(\frac{\rho_1}{\rho_2} - 1 \right), \quad (\text{A.6})$$

where $\text{We} \equiv \rho_1 U^2 h / \sigma$, and surface tension σ is assumed to be nearly constant because of the nearly constant interface temperature. Because of smallness of surface tension force components and viscous stress components relative to the interfacial pressures, Eq. (A.6) with constant $\sigma = \sigma(T_s(p_2^i)) = \sigma(T_s(p_0))$ is adequate.

- The tangential component of momentum balance at any point on the interface reduces to:

$$\mathbf{S}^i = \mathbf{S}_1^i \hat{\mathbf{n}} \cdot \hat{\mathbf{t}} = \mathbf{S}_2^i \hat{\mathbf{n}} \cdot \hat{\mathbf{t}} + \nabla_s \sigma \cdot \hat{\mathbf{t}} \quad (\text{A.7})$$

The tangential component of momentum balance at the interface, as given by Eq. (A.7), becomes:

$$\left. \frac{\partial u_1}{\partial y} \right|^i = \frac{\mu_2}{\mu_1} \left. \frac{\partial u_2}{\partial y} \right|^i + [\text{term}], \quad (\text{A.8})$$

where the term [t] in Eq. (A.8) is defined as

$$[\text{term}] = \left\{ \frac{\mu_2}{\mu_1} \left. \frac{\partial v_2}{\partial x} \right|^i - \left. \frac{\partial v_1}{\partial x} \right|^i \right\} + \frac{2\delta_x}{[1 - \delta_x^2]} \left\{ \left. \frac{\partial u_1}{\partial x} \right|^i - \left. \frac{\partial v_1}{\partial y} \right|^i \right\} - \frac{2\delta_x}{[1 - \delta_x^2]} \frac{\mu_2}{\mu_1} \left\{ \left. \frac{\partial u_2}{\partial x} \right|^i - \left. \frac{\partial v_2}{\partial y} \right|^i \right\} + \text{Ma} \left. \frac{\partial \pi_2}{\partial x} \right|^i \cdot \frac{1}{\sqrt{1 + \delta_x^2}}. \quad (\text{A.9})$$

where the Marangoni number $\text{Ma} \equiv \rho_2 U c_1 d_1 / \mu_1$ represents the surface tension contribution to tangential stress under the notation $c_1 \equiv dT_s/dp$ and $d_1 \equiv -d\sigma/dT$. For the cases considered here, a representative (for R113) set of constant values of $c_1 \approx 0.0003$ K/Pa, $d_1 \approx 0.1046$ N/(m-K), and $\text{Ma} = 0.196$ in Eq. (A.9) gives the same results as simulations without the Marangoni term. Hence the last Marangoni term on the right side of Eq. (A.9) can be dropped.

- The mass-fluxes \dot{m}_{vK} and \dot{m}_{LK} as determined by kinematic restrictions imposed by interfacial values of vapor and liquid velocities are:

$$\dot{m}_{\text{VK}} \equiv -\rho_2(\mathbf{v}_2^i - \mathbf{v}_s^i) \cdot \hat{\mathbf{n}} \quad \text{and} \quad \dot{m}_{\text{LK}} \equiv -\rho_1(\mathbf{v}_1^i - \mathbf{v}_s^i) \cdot \hat{\mathbf{n}}. \quad (\text{A.10})$$

The interfacial mass flux \dot{m}_{Energy} as obtained from energy balance at a point on the interface is given by:

$$\begin{aligned} \dot{m}_{\text{Energy}} &= 1/h_{\text{fg}}[\{\mathbf{k}_1 \nabla T_1| \cdot \hat{\mathbf{n}} - \mathbf{k}_2 \nabla T_2| \cdot \hat{\mathbf{n}}\} + \frac{d\sigma}{dt} \Big|_s + \frac{1}{2} \dot{m} \{ |\mathbf{v}_1^i - \mathbf{v}_s^i|^2 - |\mathbf{v}_2^i - \mathbf{v}_s^i|^2 \} \\ &\quad + \{\mathbf{S}_1^i \hat{\mathbf{n}} \cdot (\mathbf{v}_1^i - \mathbf{v}_s^i) - \mathbf{S}_2^i \hat{\mathbf{n}} \cdot (\mathbf{v}_2^i - \mathbf{v}_s^i)\}] \\ &\cong 1/h_{\text{fg}}[\mathbf{k}_1 \frac{\partial T_1}{\partial n} \Big|_i - \mathbf{k}_2 \frac{\partial T_2}{\partial n} \Big|_i]. \end{aligned} \quad (\text{A.11})$$

The non-dimensional form of kinematic mass fluxes \dot{m}_{VK} and \dot{m}_{LK} in Eq. (A.10) become:

$$\begin{aligned} \dot{m}_{\text{LK}} &\equiv \left[u_1^i (\partial\delta/\partial x) - (v_1^i - \partial\delta/\partial\tau) \right] / \sqrt{1 + (\partial\delta/\partial x)^2}, \quad \text{and} \\ \dot{m}_{\text{VK}} &\equiv (\rho_2/\rho_1) \left[u_2^i (\partial\delta/\partial x) - (v_2^i - \partial\delta/\partial\tau) \right] / \sqrt{1 + (\partial\delta/\partial x)^2} \end{aligned} \quad (\text{A.12})$$

The non-dimensional form of \dot{m}_{Energy} in Eq. (A.11) becomes:

$$\dot{m}_{\text{Energy}} \equiv \text{Ja} / (\text{Re}_1 \text{Pr}_1) \{ \partial\theta_1/\partial n \Big|_i - (\mathbf{k}_2/\mathbf{k}_1) \partial\theta_2/\partial n \Big|_i \}, \quad (\text{A.13})$$

where $\text{Ja} \equiv C_{p1} \Delta T / h_{\text{fg}}^0$, and $h_{\text{fg}}^0 \equiv h_{\text{fg}}(T_s(p_o))$.

The dimensional and non-dimensional forms of interfacial mass balance requirements respectively become:

$$\dot{m}_{\text{LK}} = \dot{m}_{\text{VK}} = \dot{m}_{\text{Energy}} \equiv \dot{m}. \quad (\text{A.14})$$

$$\dot{m}_{\text{LK}} = \dot{m}_{\text{VK}} = \dot{m}_{\text{Energy}} \equiv \dot{m}. \quad (\text{A.15})$$

• Under the assumption of negligible non-equilibrium thermodynamic effects and, therefore, negligible interfacial resistance (a valid assumption for all x away from $x \sim 0$ because interfacial mass-flux \dot{m} rapidly drops to modest values), the interfacial temperature values satisfy:

$$T_1^i \cong T_2^i = T_s(p_2^i). \quad (\text{A.16})$$

The non-dimensional thermodynamic restriction on interfacial temperatures, as given by Eq. (A.16), becomes:

$$\theta_1^i \cong \theta_2^i = T_s(p_2^i) / \Delta T \equiv \theta_s(\pi_2^i). \quad (\text{A.17})$$

Within the vapor phase, for the refrigerants considered here, changes in absolute pressure relative to the inlet pressure are typically so small that $\theta_s(\pi_2^i) \cong \theta_s(0) \approx \text{constant}$ is a good approximation.

Boundary Conditions

The problem posed by Eqs. (A.2), (A.4), (A.6), (A.8), (A.15), and (A.17) are computationally solved subject to boundary conditions that are

- At the inlet ($x = 0, 0 \leq y \leq 1$) at any time τ :

$$\begin{aligned} u_2(0,y,\tau) &= 1 & v_2(0,y,\tau) &= 0 \\ \pi_2(0,y,\tau) &= 0 & \theta_2(0,y,\tau) &= \theta_s(0) . \end{aligned} \quad (\text{A.18})$$

- At the bottom wall ($y = 0, 0 \leq x \leq x_e$) at any time τ :

$$u_1(x,0,\tau) = 0, \quad v_1(x,0,\tau) = 0, \quad \theta_1(x,0,\tau) = \theta_w, \quad (\text{A.19})$$

where $\theta_w \equiv T_w(x)/\Delta T$ is a constant unless it is otherwise specified. In case of flow in Fig. 2, this situation arises whenever, for a given heat load, the coolant flow rate is high enough to make the coolant temperature rise negligible as it flows past the test-section.

- At the top wall ($y = 1, 0 \leq x \leq x_e$) at any time τ :

$$u_2(x,1,\tau) = 0, \quad v_2(x,1,\tau) = 0, \quad \theta_2(x,1,\tau) = \theta_s(0) . \quad (\text{A.20})$$

Furthermore, because of the nature of boundary conditions in Eqs. (A.18) – (A.20), $\theta_2(x,y,\tau) \equiv \theta_s(0)$ is assumed/prescribed to limit the discussions in this paper to the flow of saturated vapor. This is done because, for the *pure* vapor flows considered here, it is easy to verify the well-known fact that the effects of superheat (commonly in the 5 – 10 °C range) are negligible.

Exit Conditions

Any condenser section of the type shown in Fig. 1 is typically a *part* of a closed flow loop. A flow loop which maintains a steady condensing surface temperature $T_w(x)$, a constant flow rate, and a constant pressure p_o (i.e. $\pi_2 = 0$) at the inlet, may also be designed to provide: (a) specified steady exit pressure (category-I flows) which is equivalent to, for partial condensation flows, a specified value of steady exit quality Z_e (the ratio of vapor mass flow rate at exit, $x = x_e$, to vapor mass flow rate at inlet), and (b) unspecified exit pressure (category-II flows) which is equivalent to, for partial condensation flows, unspecified values of exit quality $Z_e(t)$.

Category-I flows: For this case of *specified* exit conditions, it is assumed that the exit pressure or the exit quality Z_e specifications are still such that vapor compressibility effects can be ignored. The boundary value problem (BVP) constituting of the steady governing equations and boundary conditions – including specified steady exit conditions (steady Z_e or p_{exit}) – constitutes a steady “well-posed” category I flow problem. Steady category-I flow solutions of the governing equations, obtained by dropping all time dependencies in all the relevant equations, and solving the resulting steady equations (which are *elliptic*) for steady prescribed values of Z_e are presented here. The prescription of Z_e within $0 < Z_e < 1$ is arbitrary except that it should be such that a steady computational solution in the assumed stratified/annular regime be feasible.

The initial boundary value problem (IBVP) for the unsteady governing equations with arbitrary initial guesses under specified steady exit conditions are also “well-posed.” These solutions are supposed to be such that they get attracted, as $\tau \rightarrow \infty$, to the corresponding steady solution. If not, the unsteady solutions’ behavior at large τ indicates the stability of the corresponding steady solution. Such stability analyses are reported, for $h \rightarrow \infty$ external flow problems of Nusselt [21] and Koh [29], in Phan

and Narain ([28]) and Kulkarni et al. ([2]-[3]). Such stability analyses for steady internal category I flows, however, are not currently available and are the subjects of forthcoming papers.

An inspection of all the non-dimensional governing equations, interface conditions, and boundary conditions reveal the fact that, for category I flows, the flow is affected by the following set of non-dimensional parameters:

$$\{\text{Re}_{\text{in}}, \text{Ja}, \text{Fr}_x^{-1}, \frac{\rho_2}{\rho_1}, \frac{\mu_2}{\mu_1}, \text{Pr}_1, x_c, Z_c, \text{We}, \text{Fr}_y^{-1}\}, \quad (\text{A.21})$$

where $\text{Re}_{\text{in}} \equiv \rho_2 U h / \mu_2 \equiv \text{Re}_2$. Here Re_{in} , Fr_x^{-1} , and Ja are control parameters associated with inlet speed U , channel inclination α that determines the components of gravitational acceleration, and temperature difference ΔT . Clearly the value of Z_c or exit pressure is important for this problem. The density ratio ρ_2/ρ_1 , viscosity ratio μ_2/μ_1 , and Prandtl number Pr_1 are passive fluid parameters. Also, for unsteady or quasi-steady wavy-interface situations, the above equations imply additional dependences on a surface tension parameter, Weber number $\text{We} \equiv \rho_1 U^2 h / \sigma$, and a transverse gravity parameter $\text{Fr}_y^{-1} \equiv g_y h / U^2$. For superheated vapors, there is a very weak dependence, through Eq. (A.13), on the thermal conductivity ratio k_2/k_1 .

Category-II flows: For these flows, no exit conditions are prescribed. The steady governing equations and the remaining boundary conditions constitute an “ill-posed” boundary value problem (BVP) and no unique solution is possible. However, when unsteady category-II flows are considered for suitable initial condition choices, the initial boundary value problems (IBVP) are ‘well-posed.’ However, in general, as $\tau \rightarrow \infty$, no well-defined steady solution may exist. If they do, as is the case for gravity driven flows, one obtains a unique well defined “attracting” solution that is independent of initial guesses and one also obtains a corresponding unique exit condition $Z_c(\tau) \rightarrow Z_{c|\text{Na}}$ as $\tau \rightarrow \infty$. The stability of these attracting flows to initial disturbances has been extensively considered in [4] – [6]. For shear driven internal flows in this category, the existence or non-existence of “attractors” follow the pattern discussed for Fig. 3.

Note $\tau = 0$ cannot be chosen to be the time when saturated vapor first comes in contact and condenses on a dry sub-cooled ($T_w(x) < T_s(p_0)$) bottom plate. This is because the above described *continuum* equations will not apply at early times ($\tau \sim 0$) because inter-molecular forces will be important for very thin (approximately over 10 - 100 nm of film thickness) condensate film $\delta(x, \tau)$. Because of the above modeling limitations, the strategy here is to start at $\tau = 0$, with *any* sufficiently thick guess and look at the long time $\tau \rightarrow \infty$ behavior of the solution. Most of the time, for $\tau = 0$ initial guess, we choose *steady* solution of a category-I flow. That is, if $\phi(x, y, \tau)$ is any variable (such as u_I , v_I , π_I , θ_I , etc.), the initial values of ϕ and film thickness $\delta(x, \tau)$ are such that:

$$\phi(x, y, 0) = \phi_{\text{steady}}(x, y) \quad \text{and} \quad \delta(x, 0) = \delta_{\text{steady}}(x), \quad (\text{A.22})$$

where ϕ_{steady} and δ_{steady} are solutions of the category-I problem for a certain exit condition (exit quality Z_c or exit pressure).

9. ACKNOWLEDGMENT

This work was supported by the NSF grant CTS-0086988 and NASA grant NNC04GB52G.

10. REFERENCES

1. Narain, A., J. H. Kurita, M. Kivisalu, A. Siemionko, S. Kulkarni, T. Ng, N. Kim, and L. Phan, Oct. 2007, "Internal Condensing Flows inside a Vertical Pipe – Experimental/Computational Investigations of the Effects of Specified and Unspecified (Free) Conditions at Exit," *Journal of Heat Transfer*, Vol. 129, pp. 1352-1372.
2. S. D. Kulkarni, A. Narain, S. Mitra, and L. Phan, 2008, "Forced Flow of Vapor Condensing over a Horizontal Plate (Problem of Cess and Koh*) Part I – Steady Solutions of the Full 2D Governing Equations," Being submitted by Oct. 10, '07 (after good IMECE07 reviews) for publication in *ASME Journal of Heat Transfer*.
3. S. D. Kulkarni, A. Narain, and S. Mitra, 2008, "Forced Flow of Vapor Condensing over a Horizontal Plate (Problem of Cess and Koh*) Part II – Unsteady Solutions of the Full 2D Governing Equations Yielding Steady "Attractors" and their Unsteady Responses to Initial Disturbances and Noise," Being submitted by Oct. 10, '07 (after good IMECE07 reviews) for publication in *ASME Journal of Heat Transfer*.
4. Narain, A., Q. Liang, G. Yu, and X. Wang, Jan. 2004, "Direct Computational Simulations for Internal Condensing Flows and Results on Attainability/Stability of Steady Solutions, their Intrinsic Waviness, and Their Noise-sensitivity," *Journal of Applied Mechanics*, Vol. 71, pp. 69-88.
5. Liang, Q., X. Wang, and A. Narain, October 2004, "Effect of Gravity, Shear and Surface Tension in Internal Condensing Flows - Results from Direct Computational Simulations." *ASME Journal of Heat Transfer*, 126 (5), pp. 676-686.
6. Phan, L., X. Wang, and A. Narain, 2006, "Exit condition, Gravity and Surface-Tension Effects on Stability and Noise Sensitivity Issues for Steady Condensing Flows inside Tubes and Channels," *International Journal of Heat and Mass Transfer*, Vol. 49, Issues 13-14, pp.2058-2076.
7. Goodykoontz, J. H. and R. G. Dorsch, 1966, "Local heat transfer coefficients for condensation of steam in vertical down flow within a 5/8-inch-diameter tube," NASA TN D-3326.
8. Goodykoontz, J. H. and R. G. Dorsch, 1967, "Local heat transfer coefficients and static pressures for condensation of high-velocity steam within a tube," NASA TN D-3953.
9. Carpenter, F. G., 1948, "Heat transfer and pressure drop for condensing pure vapors inside vertical tubes at high vapor velocities," Ph. D. thesis, University of Delaware.
10. Yu, G., 1999, "Development of a CFD Code for Computational Simulations and Flow Physics of Annular/Stratified Film Condensation Flows," *Ph.D. Thesis*, ME-EM Department, Michigan Technological University.
11. Rabas, T. J., and B. Arman, 2000, "Effects of the Exit Condition on the Performance of In-Tube Condensers," *Heat Transfer Engineering*, 21(1), pp. 4-14.
12. Wedekind, G. L. and B. L. Bhatt, 1977, "An Experimental and Theoretical Investigation in to Thermally Governed Transient Flow Surges in Two-Phase Condensing Flow," *ASME Journal of Heat Transfer* 99 (4), pp. 561 – 567.
13. Bhatt, B. L. and G. L. Wedekind, 1980, "Transient and Frequency Characteristics of Two-Phase Condensing Flows: With and Without Compressibility," *ASME Journal of Heat Transfer* 102 (3), 495-500.
14. Bhatt, B. L. and G. L. Wedekind, 1980b, "A Self Sustained Oscillatory Flow Phenomenon in Two-

- Phase Condensing Flow Systems,” *ASME Journal of Heat Transfer* 102 (4), 695-700.
15. Wedekind, G. L. and B. L. Bhatt, 1989, “ Modeling the Thermally Governed transient Flow Surges in Multitube Condensing Flow Systems with Thermal Flow Distribution Asymmetry,” *ASME Journal of Heat Transfer* 111 (3), pp. 786 –791.
 16. Bhatt, B. L., G. L. Wedekind, and K. Jung, 1989, “ Effects of Two-phase pressure Drop on the Self-Sustained Oscillatory Instabilty in Condensing Flow,” *ASME Journal of Heat Transfer* 111, 538-545.
 17. Boyer, D. B., G. E. Robinson, and T. G. Hughes, 1995, “Experimental Investigation of Flow Regimes and Oscillatory Phenomena of Condensing Steam in a Single Vertical Annular Passage,” *International Journal of Multiphase Flow*, Vol. 21, No. 1, pp. 61 – 74.
 18. Wedekind, G. L., C. J. Kobus, and B. L. Bhatt, 1997, “Modeling the Characteristics of Thermally Governed Transient Flow Surges in Multitube Two-Phase Condensing Flow Systems with Compressibility and Thermal and Flow Distribution Asymmetry,” *ASME Journal of Heat Transfer*, Vol. 119, No. 3, pp. 534 – 543.
 19. Kobus, C. J., G. L. Wedekind, and B. L. Bhatt, 2000, “Predicting the Influence of Compressibility and Thermal and Flow Distribution Asymmetry on the Frequency-Response Characteristics of Multitube Two-Phase Condensing Flow Systems,” *ASME Journal of Heat Transfer*, Vol. 122, No. 1, pp. 196 – 200.
 20. Patankar, S. V., 1980, *Numerical Heat Transfer and Fluid Flow*, Hemisphere, Washington D. C. *Journal of Multiphase Flow*, Vol. 16, pp. 139 – 151.
 21. Nusselt, W., 1916, “Die Oberflächenkondensation des Wasserdampfes,” *Z. Ver. Dt. Ing.* 60 (27), pp. 541-546.
 22. Narain, A. and Y. Kizilyalli, 1991, “Pressure driven flow of pure vapor undergoing laminar film condensation between parallel plates,” *International Journal of Non-Linear Mechanics*, Vol. 26, No. 5, pp. 501-520.
 23. Narain, A., G. Yu, and Q. Liu, 1997, “Interfacial Shear Models and Their Required Asymptotic Form for Annular Film Condensation Flows in Inclined Channels and Vertical Pipes,” *International Journal of Heat and Mass Transfer*, Vol. 40, NO. 15, pp. 3559 - 3575.
 24. Garimella, S., J. D. Killion, and J. W. Coleman, 2002 “An Experimentally Validated Model for Two-Phase Pressure Drop in the Intermittent Flow Regime for Circular Microchannels,” *Journal. of Fluids Engineering*, Vol. 124, pp. 205-214.
 25. Garimella, S., J. D. Killion, and J. W. Coleman, 2003 “An Experimentally Validated Model for Two-Phase Pressure Drop in the Intermittent Flow Regime for Non-Circular Microchannels,” *Journal of Fluids Engineering.*, Vol. 125, pp. 887-894
 26. Liao, N. S., C. C. Wang, and C. L. Tien, 1988, "Analysis of Transient Flow Surge Phenomena in a Single-Tube Condenser,” *International Communications in Heat and Mass Transfer*, Vol. 15, pp. 257 – 268.
 27. Liao, N. S. and C. C. Wang, 1990, “Transient response Characteristics of Two-Phase Condensing Flows,” *International Journal of Multiphase Flow*, Vol. 16, 139-151.
 28. Phan, L. and A. Narain, 2007, “Non-linear Stability of the Classical Nusselt problem of Film Condensation and Wave Effects,” *ASME Journal of Applied Mechanics*, Vol.74, No.2, pp. 279-290.
 29. Koh, J. C. Y., 1962, “Film Condensation in a Forced-Convection Boundary-Layer Flow,” *International Journal of Heat and Mass Transfer*, Vol. 5, pp. 941-954.
 30. Palen, J. W., R. S. Kistler, and Y. Z. Frank, 1993, “What We Still Don’t Know About Condensation in Tubes,” In *Condensation and Condenser Design* (Edited by J. Taborek, J. Rose and I. Tanasawa), Pub.: United Engineering Trustees, Inc. for Engineering Foundation and ASME, New York, pp. 19–

53.

31. Ng, T. W., 2006, "Development and Calibration of a Fluorescence and Fiber-Optics Based Real-Time Thickness Sensor for Dynamic Liquid Films," *Ph.D. Thesis*, MEEM, Michigan Technological University.
32. Siemonko, A., 2006, "Design, Fabrication, and Operation of a System to Control FC-72 Condensation Inside a Vertical Tube," *Ph.D. Thesis*, Chem Eng, Michigan Technological University.
33. Kurita, J. H., 2006, "Experimental Investigation of Fully Condensing Downward Vapor Flows in a Vertical Tube - Unspecified (Free) Exit Condition Cases," *M. S. Thesis*, MEEM, Michigan Technological University.
34. Narain, A., J. H. Kurita, M. Kivisalu, A. Siemionko, S. Kulkarni, T. Ng., N. Kim, and L. Phan, Jan 2007, "Internal Condensing Flows inside a Vertical Pipe – Experimental/Computational Investigations of the Effects of Specified and Unspecified (Free) Exit Conditions at Exit," A Technical Report which is an extended version of ref. [1] and is available at: <http://www.me.mtu.edu/~narain/narainpublications1.htm>
35. Parratt, L. G., 1961, *Probability and Experimental Errors in Science – An Elementary Survey*, Wiley, New York.
36. Carey, V. P., 1992, *Liquid-Vapor Phase-Change Phenomena*, Series in Chemical and Mechanical Engineering, Hemisphere Publishing Corporation, New York.
37. Lu, Q. and N. V. Suryanarayana, 1995, "Condensation of a Vapor Flowing Inside a Horizontal Rectangular Duct," *Journal of Heat Transfer*, 117, pp. 418-424.
38. Hewitt, G. F., Shires, G. L., and Bott, T. R., 1994, *Process Heat Transfer*, CRC Press, Inc., Begall House, Boca Raton, Florida.
39. Lockhart, R. W. and Martinelli, R.C., 1949, "Proposed Correlation of Data for Isothermal Two-Phase two-component flow in a pipe," *Chem. Eng. Prog.*, 45, No. 1, pp. 39–48.
40. Taitel, Y. and Dukler, A. E., 1976, "A Model for predicting Flow regime transition in horizontal and near horizontal gas-liquid flow," *AIChE Journal*, 22, pp. 47-55.
41. Chen, J. C., 1966, "Correlation for boiling heat transfer to saturated fluids in convective flow," *Ind. Chem. Eng. Proc. Design and Dev.*, 5, pp. 322-339.
42. McDermott, B. and Timothy Shedd, "Detailed Pressure Drop and Flow Regime Characteristics of Adiabatic Two-Phase Flow of Pure Refrigerant R-123," Paper no. IMECE2007-43829, Proceedings (CD ROM) of ASME, IMECE 2007, Seattle, Nov. 11-15, 2007.
43. Delhaye, J. M., 1974, "Jump Conditions and Entropy Sources in Two-phase Systems; Local Instant Formulation," *Int. J. of Multiphase Flow*, 1, pp. 395-409.